

2

MICROWAVE LABORATORY REPORT NO. 90-P-4

**MICROWAVE AND MILLIMETER-WAVE OSCILLATORS
AND PLANAR POWER COMBINING STRUCTURES
FOR QWITT AND GUNN DIODES**

TECHNICAL REPORT

AMIR MORTAZAWI, DEAN NEIKIRK AND TATSUO ITOH

AUGUST 1990

REC
AUG 29 1990
D

**UNITED STATES ARMY RESEARCH OFFICE
CONTRACT NUMBER DAAL03-88-K-0005**

**JOINT SERVICES ELECTRONICS PROGRAM
RESEARCH CONTRACT AFSOR F49620-89-C-0044**

**THE UNIVERSITY OF TEXAS AT AUSTIN
DEPARTMENT OF ELECTRICAL AND COMPUTER
ENGINEERING**

AUSTIN, TEXAS 78712

DISTRIBUTION STATEMENT A
Approved for public release;
Distribution Unlimited

SECURITY CLASSIFICATION OF THIS PAGE

REPORT DOCUMENTATION PAGE

1a. REPORT SECURITY CLASSIFICATION Unclassified		1b. RESTRICTIVE MARKINGS	
2a. SECURITY CLASSIFICATION AUTHORITY		3. DISTRIBUTION/AVAILABILITY OF REPORT Approved for public release; distribution unlimited.	
2b. DECLASSIFICATION/DOWNGRADING SCHEDULE		4. PERFORMING ORGANIZATION REPORT NUMBER(S) Microwave Laboratory Report No. 90-P-4	
5. MONITORING ORGANIZATION REPORT NUMBER(S) ARO 25045.44-EL		6a. NAME OF PERFORMING ORGANIZATION The University of Texas	
6b. OFFICE SYMBOL (if applicable)		7a. NAME OF MONITORING ORGANIZATION U. S. Army Research Office	
6c. ADDRESS (City, State, and ZIP Code) Dept. of Electrical & Computer Engineering Austin, Texas 78712		7b. ADDRESS (City, State, and ZIP Code) P. O. Box 12211 Research Triangle Park, NC 27709-2211	
8a. NAME OF FUNDING/SPONSORING ORGANIZATION U. S. Army Research Office		8b. OFFICE SYMBOL (if applicable)	
8c. ADDRESS (City, State, and ZIP Code) P. O. Box 12211 Research Triangle Park, NC 27709-2211		9. PROCUREMENT INSTRUMENT IDENTIFICATION NUMBER	
10. SOURCE OF FUNDING NUMBERS		11. TITLE (Include Security Classification) Microwave and Millimeter-Wave Oscillators and Planar Power Combining Structures for QWITT and Gunn Diodes	
PROGRAM ELEMENT NO.		PROJECT NO.	
TASK NO.		WORK UNIT ACCESSION NO.	
12. PERSONAL AUTHOR(S) Amir Mortazawi, Dean Neikirk and Tatsuo Itoh			
13a. TYPE OF REPORT Technical		13b. TIME COVERED FROM _____ TO _____	
14. DATE OF REPORT (Year, Month, Day) 1990, August		15. PAGE COUNT 103	
16. SUPPLEMENTARY NOTATION The view, opinions and/or findings contained in this report are those of the author(s) and should not be construed as an official Department of the Army position, policy, or decision, unless so designated by other documentation.			
17. COSATI CODES		18. SUBJECT TERMS (Continue on reverse if necessary and identify by block number)	
FIELD	GROUP	SUB-GROUP	Quantum well oscillators, QWITT diode, power combining, quasi optical power combining
19. ABSTRACT (Continue on reverse if necessary and identify by block number) Quantum well (QW) diode oscillators have recently been shown to have the potential to generate power in the millimeter (mm) and sub-mm wave region. The small signal microwave impedance of a modified QW device called the quantum well injection transit time (QWITT) diode is measured and compared with theoretical predictions. Based on the small signal impedance of the device, several QWITT oscillators were designed and fabricated. The highest power ever reported for a QW diode oscillator was obtained at about 8 GHz.			
20. DISTRIBUTION/AVAILABILITY OF ABSTRACT <input checked="" type="checkbox"/> UNCLASSIFIED/UNLIMITED <input type="checkbox"/> SAME AS RPT. <input type="checkbox"/> DTIC USERS		21. ABSTRACT SECURITY CLASSIFICATION Unclassified	
22a. NAME OF RESPONSIBLE INDIVIDUAL Tatsuo Itoh		22b. TELEPHONE (Include Area Code) (512) 471-1072	
		22c. OFFICE SYMBOL	

ABSTRACT

Quantum well (QW) diode oscillators have recently been shown to have the potential to generate power in the millimeter (mm) and sub-mm wave region. The small signal microwave impedance of a modified QW device called the quantum well injection transit time (QWITT) diode is measured and compared with theoretical predictions. Based on the small signal impedance of the device, several QWITT oscillators were designed and fabricated. The highest power ever reported for a QW diode oscillator was obtained at about 8 GHz.

Due to the strong nonlinearity of the QWITT diode, mixers can also be constructed using this device. A waveguide and a planar QWITT diode self-oscillating mixer were tested. These mixers, for the first time, achieved conversion gain.

Even though QW devices are capable of operation at mm and sub-mm wave frequencies, the power they generate is small. A periodic planar power combining structure is described that can combine power generated from several negative resistance devices. Because of the periodicity of the structure, there is no need for an external resonator and therefore the structure is compatible with monolithic fabrication. Experimental tests were carried out of the structure using Gunn diodes. In some cases power combining efficiencies higher than 100% were obtained.

The frequency of operation of QW diodes can be expanded by using them as harmonic generators. In this case also a power combining technique is required to

increase the harmonic power generated to a useful level. Several negative resistance devices are injection locked at the fundamental frequency. Second harmonic is generated due to the device nonlinearity and is radiated out into space through an array of microstrip patch antennas. Therefore the second harmonic power generated by several devices is combined in space. Experimental results of a second-harmonic combiner using Gunn diodes are presented.

Allocation For	
CLASS CRA&I	<input checked="" type="checkbox"/>
CLASS TAB	<input type="checkbox"/>
Unprocessed	<input type="checkbox"/>
Classification	
Distribution/	
Availability Codes	
Avail and/or	
Dist Special	
A-1	



TABLE OF CONTENTS

Chapter 1.	INTRODUCTION	1
Chapter 2.	SMALL SIGNAL IMPEDANCE MEASUREMENT OF THE QWITT DIODE AND COMPARISON BETWEEN THEORY AND EXPERIMENT	5
	2.1 Small Signal QWITT Diode Model	6
	2.2 Experiment	11
	2.3 Results	17
	2.4 Determination of an Upper Limit for the Oscillation Frequency of QWITT Diode	22
	2.5 Discussion and Conclusion	26
Chapter 3.	QWITT DIODE OSCILLATORS SMALL SIGNAL ANALYSIS AND DESIGN	27
	3.1 Negative Resistance Oscillator Design	27
	3.2 Design of Planar QWITT Diode Oscillators	35
	3.3 Experimental Results for Planar QWITT Diode Oscillators	37
	3.4 Attempts to Design a 94 GHz QWITT Diode Oscillator	47
	3.5 Conclusion	51
Chapter 4.	SELF OSCILLATING QWITT DIODE MIXERS	52
	4.1 Basic Mixer Theory	52
	4.2 Experimental Results and Discussion	54
	4.3 Conclusion	60
Chapter 5.	A PERIODIC POWER COMBINING STRUCTURE	62
	5.1 Theory	63

	5.2	Large Signal Impedance Determination	67
	5.3	Design Procedure	69
	5.4	Experiment and Results	71
	5.5	Conclusion	76
Chapter 6.		SECOND HARMONIC QUASI-OPTICAL POWER COMBINERS AND TRANSCEIVERS	77
	6.1	Theory	78
	6.2	Circuit Description	82
	6.3	Design	85
	6.4	Experiment	88
	6.5	Conclusion	96
Chapter 7.		CONCLUSIONS	97
References			99

CHAPTER 1

INTRODUCTION

In recent years there has been a new interest in millimeter wave technology. Vacuum tube sources that cover the entire millimeter wave spectrum exist but there is a demand for solid state devices capable of operation at millimeter and sub-millimeter wave frequencies. There are solid state sources such as Impatt and Gunn diodes that can operate in the lower millimeter wave region but their efficiency and performance degrade at higher frequencies.

Quantum well devices have recently been shown to be capable of generating power at millimeter and sub-millimeter wave frequencies [1]-[3]. This is because the intrinsic negative resistance region for the quantum well device extends from DC up to several hundred GHz. Quantum well devices are also very attractive because quantum mechanical tunneling is intrinsically a low noise process. However, the output power obtained from these devices, thus far, has been rather low. The physical device structures that must be used to maximize the output power density obtained from these devices remain to be explored fully.

A modified version of quantum well device, the quantum well injection transit time (QWITT) diode, consisting of a double barrier structure coupled with a depletion region or drift region, was proposed by Kesan et al. [4]. This device exploits transit time phenomena to improve the output power of the conventional quantum well devices.

In the second chapter of this work, the small signal impedance measurement of the microwave impedance of the QWITT diode is described. The experimental results

are compared with the theoretical calculations [5]. Based on the measurements, the maximum operating frequency of the QWITT diode is determined.

In the third chapter, the design of negative resistance oscillators based on small signal analysis is described. Then design and experiments concerning several planar QWITT diode oscillators are discussed. These oscillators are designed based on the small signal information described in Chapter 2. The planar QWITT diode oscillator generated the highest power ever reported from a quantum well device. Also some of the author's attempts in making a 94 GHz QWITT diode oscillator are mentioned.

Due to the strong nonlinearity of the quantum well diode in the region of negative resistance, it has a potential to make an efficient self-oscillating mixer. In the fourth chapter some experimental results obtained from a waveguide and a planar self-oscillating mixer using QWITT diodes are presented. These mixers operate in the X-band region. The wave guide mixer operates in the third harmonic conversion mode and the planar mixer operates in the fundamental mode. It is shown that both of these self oscillating mixers can achieve conversion gain in a very narrow band of intermediate frequency. Broad band operation also is possible which results in some conversion loss.

Even though the QWITT diode has capability to produce higher power than the quantum well diode, for most of applications in the millimeter and sub-millimeter wave region, there is still a need for more power. In general, power combining structures can be used to combine power generated from several QWITT diode oscillators. The conventional power combining structures are bulky and complicated. It is very desirable to design power combiners having simple structures compatible with

monolithic fabrication. In the fifth chapter, a periodic planar power combining structure is introduced. Since the periodicity of the structure determines the oscillation frequency, there is no need for an external resonator.

There is always a limit to the frequency at which a solid state oscillator can operate. In that limit, the negative resistance of the device becomes so small that it can not compensate the resonator's loss. One way to generate millimeter and sub-millimeter wave frequencies is to use a negative resistance device as harmonic generator. Even though solid state devices do not exhibit negative resistance above a certain range of frequencies, because of device nonlinearities, higher harmonics are being generated. Through proper circuit design, harmonic generation can be enhanced and then filtered out for use. One problem with this method is the low conversion efficiency. Here again we can take advantage of different power combining techniques. In general at millimeter wave frequencies quasi-optical techniques are preferred since guiding structures are lossy. Since the nonlinearity of negative resistance devices is maintained at higher harmonics they can also be used as self oscillating harmonic mixers. This type of approach can simplify the construction of transceiver modules and hence reduce their size and cost.

In Chapter six, a second harmonic quasi-optical power combining structure is discussed. Several negative resistance devices are used as harmonic generators. These devices are injection locked to each other at the fundamental frequency. Several microstrip patch antennas are used to compose an antenna array. Each of the patch antennas is integrated with an active element and radiates the second harmonic into

space. Therefore the second harmonic generated from several devices is combined in space.

Conclusions are given in the seventh chapter.

CHAPTER 2

SMALL SIGNAL IMPEDANCE MEASUREMENT OF THE QWITT DIODE AND COMPARISON BETWEEN THEORY AND EXPERIMENT

During the past several years, different small signal models for the quantum well (QW) and quantum well injection transit time (QWITT) diodes have been developed. These models are derived based on theoretical considerations from a solid state point of view. There are many advantages that we can gain from experimental determination of the small signal impedance of the device. First, different theoretical models can be verified and their shortcomings can be investigated. Second, information about the small signal impedance of the device can be used for proper circuit design. Third, using this information, lumped element models for the device can be constructed and parasitics like series resistance which put an upper limit to operation frequency can be identified. This information can help us to determine different problems associated with the device fabrication such as large series resistance due to ohmic contacts and so on. Therefore determining a reliable model for the device can help us to modify the fabrication procedure to make a better device.

In the past, there have been attempts to model resonant tunneling diodes by constructing an equivalent circuit for the device and adjusting the circuit elements until the equivalent circuit response matches the data obtained from measurements. These equivalent circuit models have required the use of circuit elements that were not physically justified [6] and their values were determined merely by curve fitting the response of the equivalent circuit model to the experimental data.

The QWITT diode model developed by Kesan et al. [7], provides a direct calculation of the device impedance based only on DC measurements and the knowledge of the device structure. To verify this model, small signal impedance measurements of several QWITT diodes with drift region lengths of 500, 1000 and 2000 Å were performed which are presented in Section 2.2. The calculated data from the QWITT diode model are in very good agreement with the measured data.

2.1-Small Signal QWITT Diode Model

Small signal modeling of the QWITT diode is based on a paper by Kesan et al. [7]. The structure that is analyzed is shown in Fig. 2.1. It is assumed that the length of the quantum well region (L) is much smaller than the depleted spacer layer W . For the small signal analysis the quantum well is characterized by the normalized injection conductance σ .

$$\sigma = L \left(\frac{\partial J_{QW}}{\partial V_{QW}} \right)_{V_0} \quad (2.1)$$

J_{QW} is the instantaneous current density and V_{QW} is the instantaneous voltage across the quantum well region measured at the DC bias voltage V_0 which is also applied only across the quantum well region. The impedance of the quantum well region as a function of frequency can be calculated by

$$Z_{QW} = \frac{L}{\sigma + j\omega\epsilon'} \quad (2.2)$$

where ϵ' is the effective dielectric constant of the quantum well region.

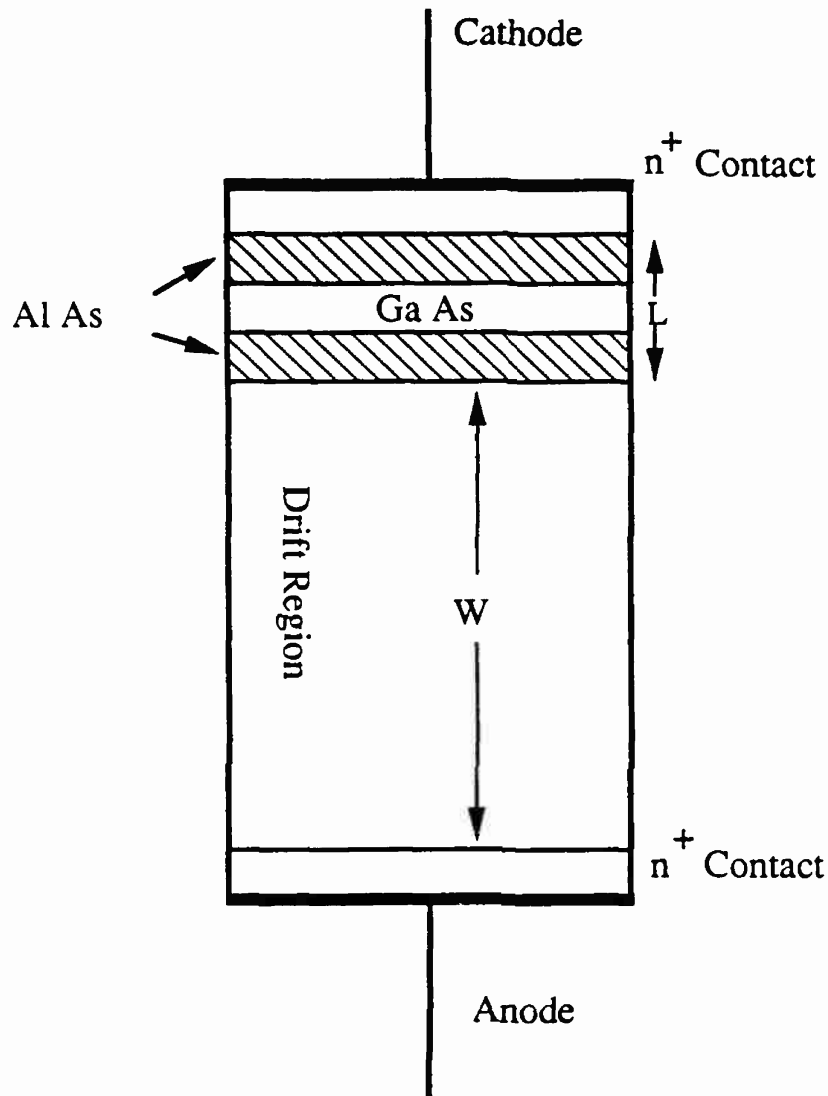


Fig. 2.1 QWITT diode structure. A thick undoped GaAs spacer layer is used on the anode side to produce a depletion region of length W , much longer than the thickness of the quantum well region L .

To determine the impedance of the drift region, the electric field across the drift region is integrated and then divided by the current through the device. It is assumed that electrons travel at their saturation velocity v_s across the drift region. The impedance of the drift region is given by

$$Z_{tt} = \frac{W}{j\omega\epsilon} \left[1 - \frac{\sigma}{\sigma + j\omega\epsilon} \frac{1 - e^{-j\theta_d}}{j\theta_d} \right] \quad (2.3)$$

where ϵ is the dielectric constant of the drift region, W is the length of the drift region, σ is the injection conductance of the quantum well and θ_d is the drift angle determined by

$$\theta_d = \frac{\omega W}{v_s} \quad (2.4)$$

The total impedance of the QWITT diode is the sum of the impedance of the quantum well and the impedance of the drift region.

$$Z_{QWITT} = Z_{QW} + Z_{tt} \quad (2.5)$$

Based on the above equations an equivalent circuit for the QWITT diode which is shown in Fig. 2.2 can be drawn. Z_{QW} is the specific impedance and ϵ' is the effective dielectric constant of the quantum well. Z_{tt} is the specific impedance of the drift region. In general, by knowing the physical dimensions of the structure and the DC I-V characteristics, and by using the small signal impedance calculation one can determine the values of lumped elements in the equivalent circuit model.

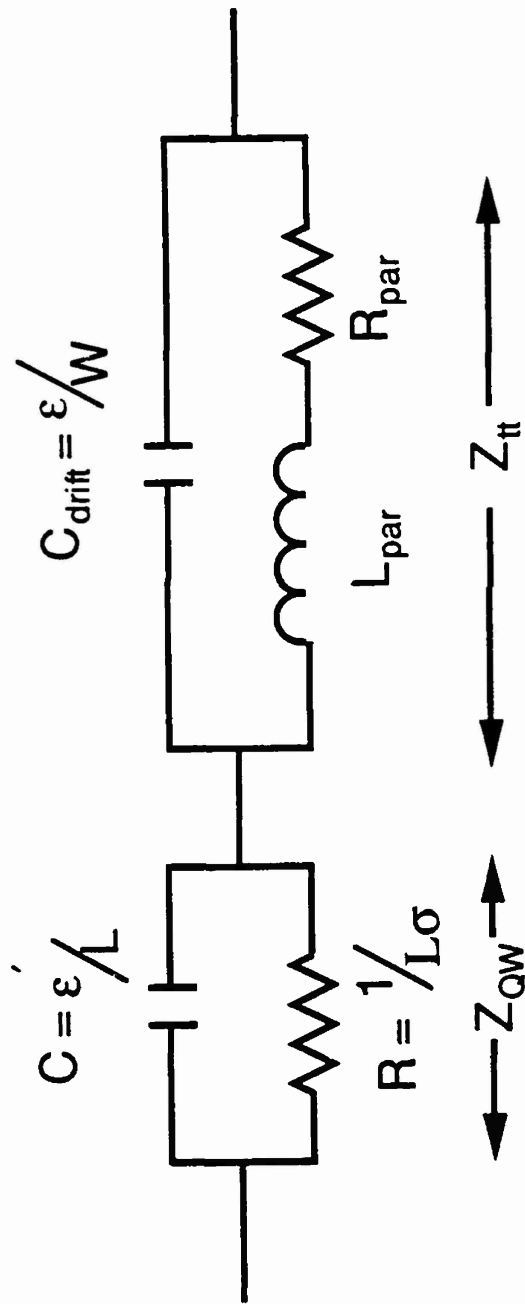


Fig. 2.2 Small signal equivalent circuit for the QWITT diode

The real part of the impedance of the drift region is given by

$$R_{it} = \frac{2 \left(\frac{v_s \epsilon}{2 \sigma^2} \right)}{\left(\frac{\omega}{\sigma/\epsilon} \right)^2 \left[1 + \left(\frac{\omega}{\sigma/\epsilon} \right)^2 \right]} \left[1 - \cos \left(\frac{\omega W}{v_s} \right) + \frac{\omega}{\sigma/\epsilon} \sin \left(\frac{\omega W}{v_s} \right) \right] \quad (2.6)$$

In order to determine the optimum length of the drift region, W , which yields the maximum negative resistance contribution from the drift region at a specific frequency of operation, we can solve the equation $\partial R/\partial W = 0$ [7].

By measuring the DC I-V curve of the QWITT diode and knowing the series resistance due to ohmic contacts, one can determine the injection conductance of the quantum well region, σ . This is done through an iterative procedure based on a simple depletion approximation [8]. After determining σ and by using the physical dimensions of the device, one can calculate the impedance of the QWITT diode at microwave frequencies.

We would like to experimentally verify the theoretical results for the impedance of the QWITT diode. Also, by comparing the measured small signal RF impedance of the QWITT diode with the theoretical calculations, one can determine the value of the parasitic series resistance. Having a complete equivalent circuit model for the device can help us to predict the upper frequency limit for the negative resistance operation which is a figure of performance for the device.

2.2-Experiment

Quantum well devices maintain their negative resistance from DC up to microwave and millimeter wave frequencies (depending on the device structure and the parasitic series resistance). Impedance measurements in the negative resistance region are very difficult. The combination of the device and measurement circuit can act as a resonant circuit. If any resonance exists in the broad range of frequencies over which the device has negative resistance, parasitic oscillations can occur. Due to the self bias condition (because of the parasitic oscillations) and the fact that the impedance of the device is a strong function of the RF voltage that appears across it, the impedance obtained by measurement can be very different from the true small signal impedance of the QWITT diode.

By looking back at the theoretical expressions for the impedance of the QWITT diode (Section 2.1), we can see that the impedance of the device can be calculated both in the negative and positive resistance region. The only parameter that determines the region of operation is the bias point. In the region of positive resistance, the sign of the injection conductance of the quantum well σ is positive and in the negative resistance region the sign of σ is negative. Since, theoretically, we are able to calculate the RF impedance of the QWITT diode in the positive resistance region as well as negative resistance region, one also can try to perform the RF impedance measurement in the positive resistance region to verify the theoretical predictions. In this case there is no need to be worried about complications that may arise from performing the measurement in the negative resistance region.

The impedance measurements were conducted using a HP8510 automatic network analyzer. The impedance measurement was performed in the range of frequencies from 50 MHz to 30 GHz. The chips that were probed were mesa isolated on an n^+ substrate. A Design Technique coplanar probe is used to probe a QWITT mesa on the substrate. Since the ground plane was on the backside of the substrate, silver epoxy was used to extend the backside ground plane into the same plane with the device mesas so that the coplanar probes could be used to perform the measurements (Fig. 2.3).

Extension of the ground plane by silver epoxy might introduce some parasitics which could alter the true impedance of the device significantly. In order to determine the parasitics introduced by silver epoxy and to de-embed them if necessary, some ohmic contacts similar to the device structures were probed. The parasitic series resistance due to the silver epoxy was determined to be negligible and also no appreciable reactive component was observed. Results of a typical measurement of an ohmic contact are shown in Fig. 2.4.

Figure 2.5 shows the cross sectional structure of the QWITT diodes used in this study. Three different QWITT diodes with drift region lengths 500 (device A), 1000 (device B) and 2000 (device C) Å were measured. Fig. 2.6 shows the DC I-V curves of three devices that were probed. The impedance measurements were performed at different bias voltages all in the positive resistance regions.

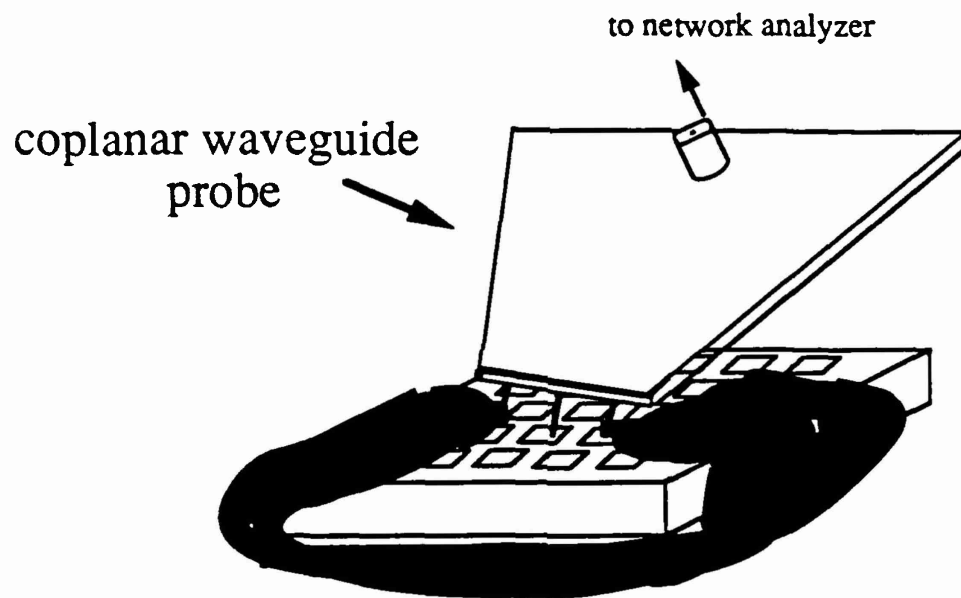


Fig. 2.3 Impedance measurement using a coplanar probe. The chip ground plane is moved to the same plane as device mesas. The output of the coplanar probe is connected to an automatic network analyzer.

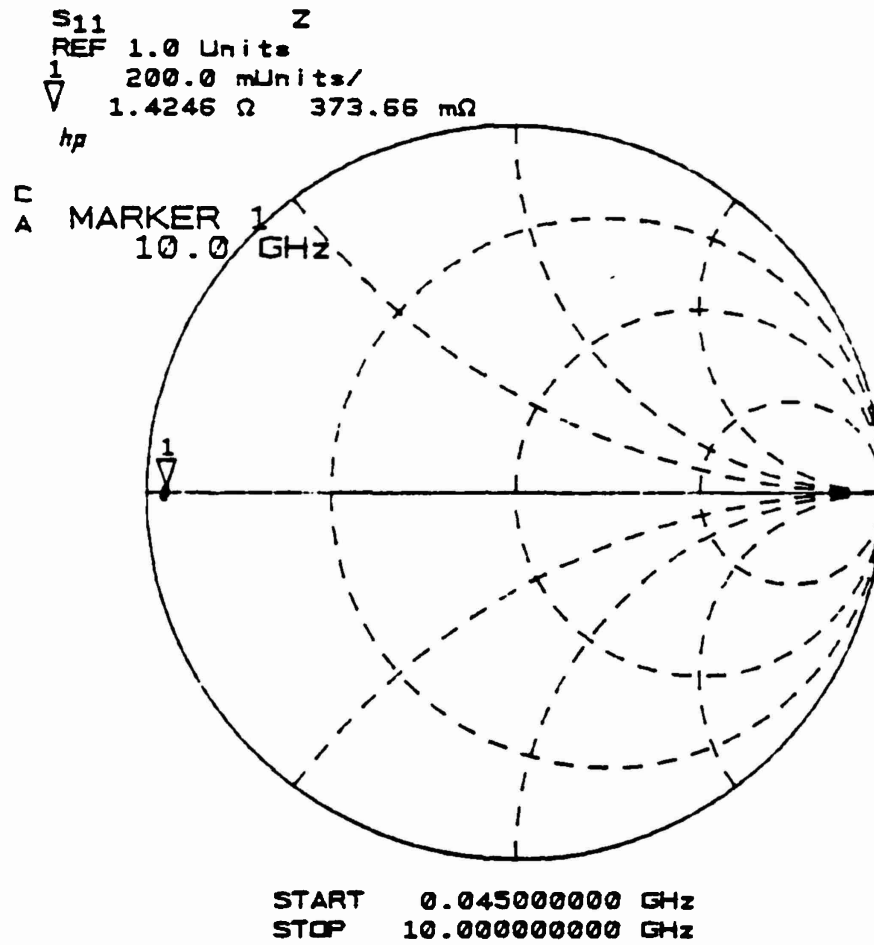


Fig. 2.4 Results obtained from impedance measurement of an ohmic contact

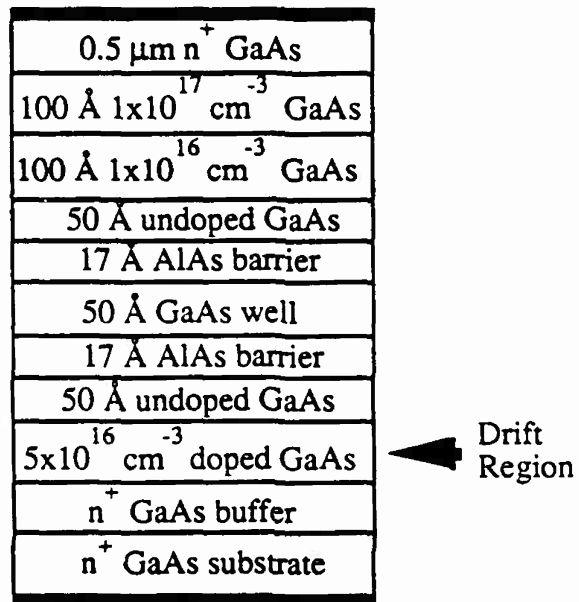


Fig. 2.5 Cross section of QWITT diode. The length of drift regions for devices A, B and C are 500, 1000 and 2000 \AA respectively.

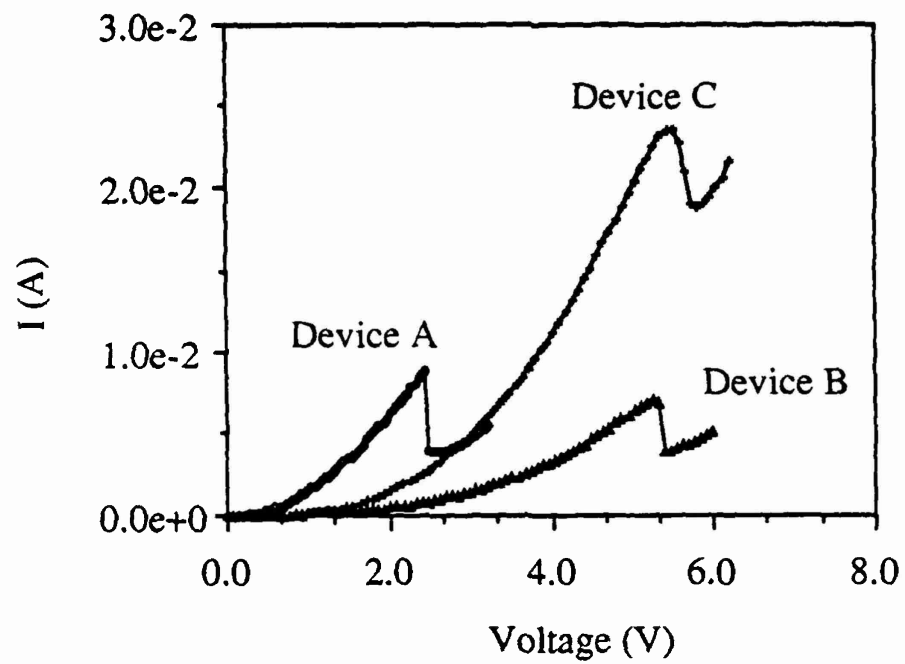


Fig. 2.6 DC I-V curves for the QWITT diodes A, B and C

2.3-Results

Comparison between measured and calculated results for several diodes at different bias points are shown in Figs. 2.7, 2.8, 2.9 and 2.10. Figure 2.7 and 2.8 show the measured impedance for device A (500 Å drift region) at two different bias points in the DC I-V curve. As was mentioned before, at each bias point the DC I-V curve, device structure, and a simple depletion approximation are used to find the injection conductance σ needed for the calculation. A series parasitic resistance is added to account for fairly large values of contact resistance (independently estimated to be in the mid $10^{-5} \Omega \text{ cm}^2$ range). The fit between model and measurement (see for example, Figs. 2.9 and 2.10) is quite good for all three device structures, over all the bias cases measured. These measurements show that the theoretical model for the QWITT diode can predict the small signal RF impedance very well. Also, based on the measured and theoretical results the parasitic series resistance associated with each device was determined.

The physical device model which allows us to predict QWITT diode impedance can also be used to determine if there is a simple equivalent circuit for the device. Using the circuit shown in Fig. 2.11 a simple equivalent circuit consisting of frequency-independent circuit elements which fit the calculated impedance quite well was found. The circuit contains a series resistor (R_s) which accounts for the ohmic contact resistance as well as the bulk resistance. The value of R_s in the equivalent circuit is determined independently (based on the estimated contact resistance). Values of all the elements except L in the equivalent circuit are determined using the small signal model [7] of the device. The capacitor C in the model is the depletion layer

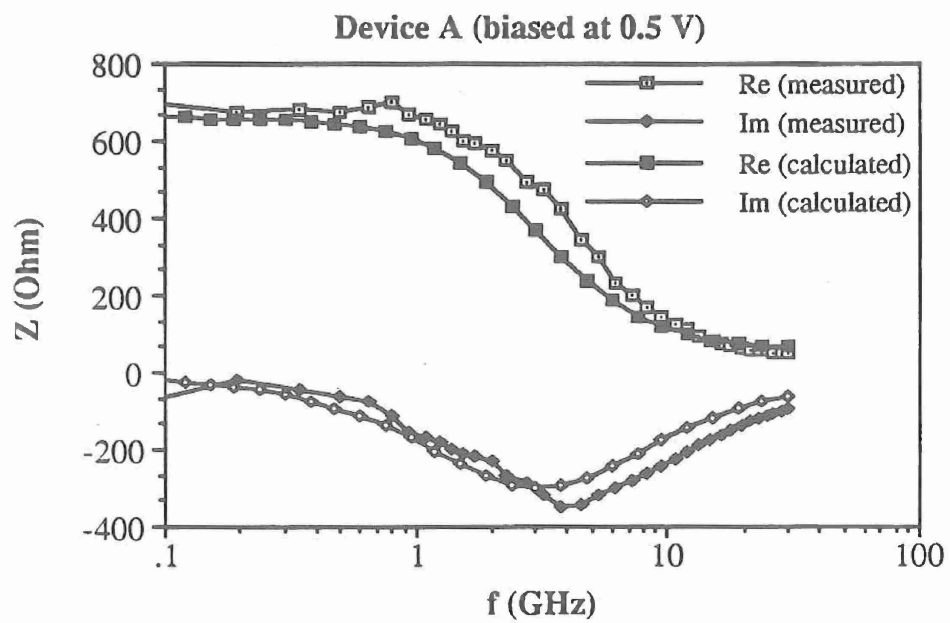


Fig. 2.7 Measured and calculated impedance of device A at 0.5 V. The device area is $52 \mu\text{m}^2$

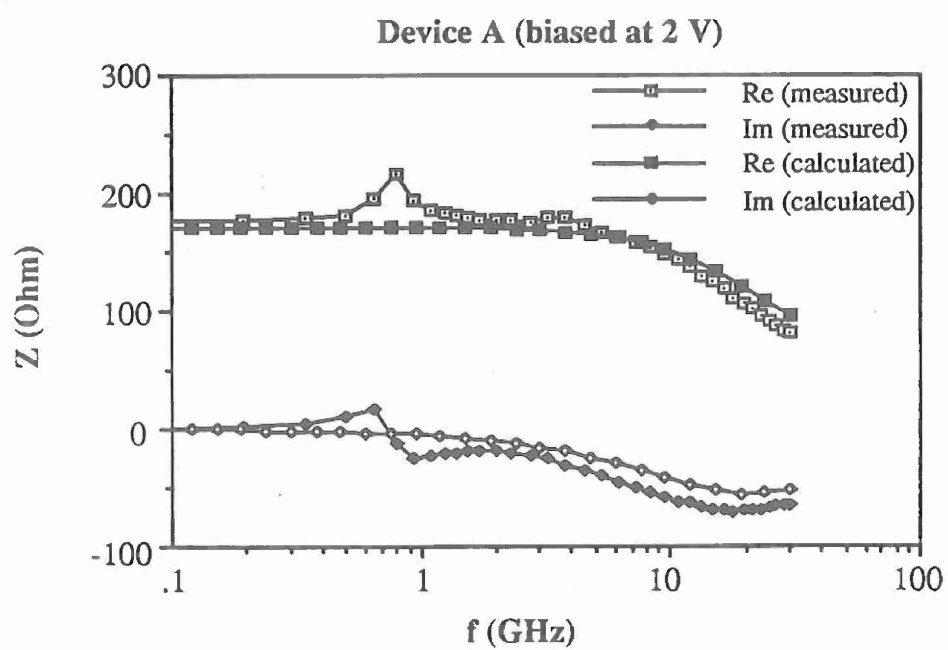


Fig. 2.8 Measured and calculated impedance of device A at 2 V. The device area is $52 \mu\text{m}^2$

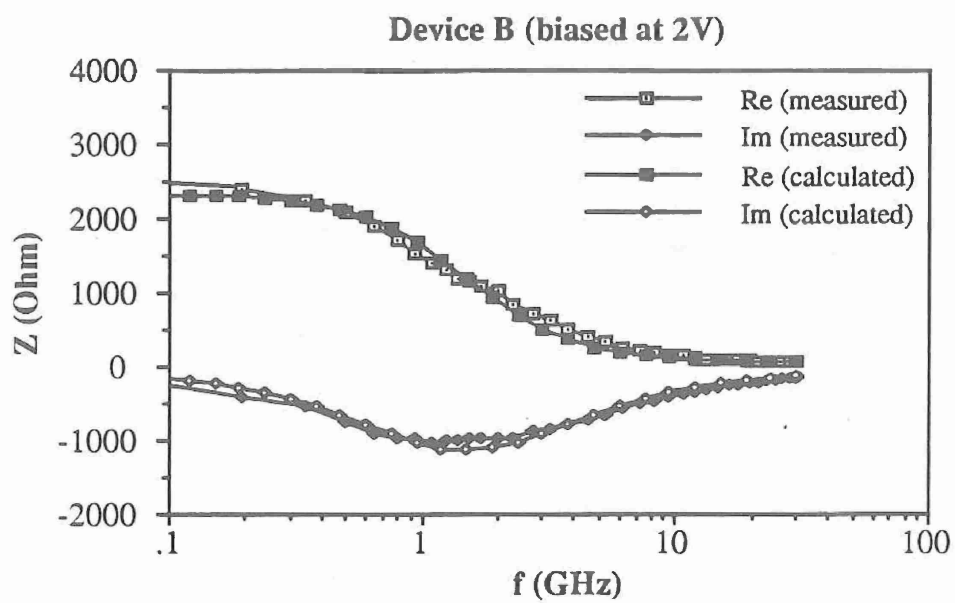


Fig. 2.9 Measured and calculated impedance of device B at 2 V. The device area is $52 \mu\text{m}^2$.

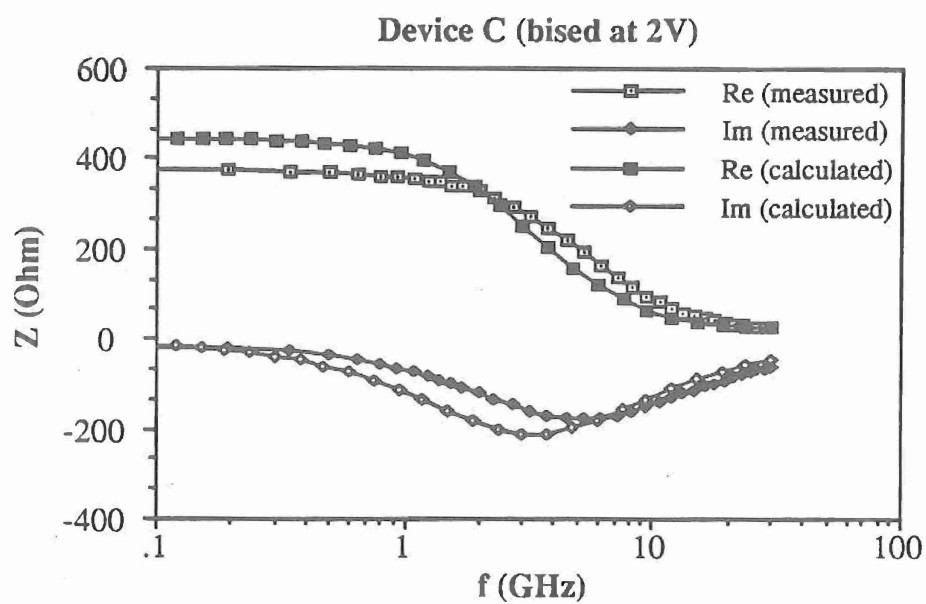


Fig. 2.10 Measured and calculated impedance of device C at 2 V. The device area is $225 \mu\text{m}^2$.

capacitance for the structure. In parallel with the capacitor is a series resistor/inductor combination (see Fig. 2.11). R is simply the overall device differential resistance measured from the DC I-V curve, after accounting for contact resistance. The inductive element L is a manifestation of space charge effects, and is a simple consequence of carrier transport across a depletion region. The value of L is determined by curve fitting the response of the lumped element equivalent circuit to measured data. It should be noted that the device model is fully classical, and that the inductive element is not due to quantum transport effects. The values of equivalent circuit elements for devices A, B and C are shown in Table 2.I.

2.4-Determination of an Upper Limit for the Oscillation Frequency of QWITT Diode

Based on the values obtained for parasitic series resistance of the QWITT diode and the slope of the DC I-V curve in the negative resistance region one can determine the impedance of the structure in the negative resistance region as a function of frequency. From this the frequency at which the real part of the impedance of the device is not negative any more can be determined. Therefore we can find an upper limit to the frequency at which a specific QWITT diode can oscillate. Fig. 2.12 shows the impedance of the device C when it is biased in the middle of its negative resistance region. From the figure, it can be seen that the real part of the impedance of the device crosses zero at about 25 GHz; therefore one can be sure that this specific device can not oscillate at frequencies higher than 25 GHz. As was mentioned, the series resistance due to the ohmic contacts can degrade the performance of the device [4]. If we reduce the series resistance of the device, R_s , by one order of magnitude, the simulation shows

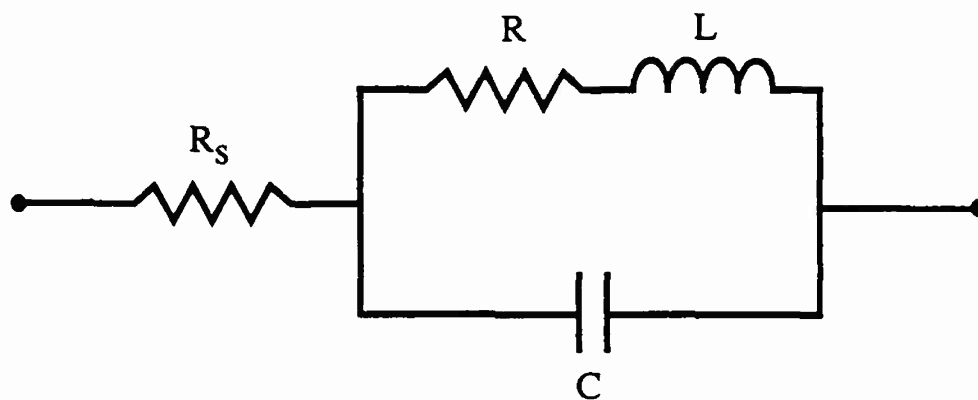


Fig. 2.11 Equivalent circuit for QWITT diode, capacitor C is the depletion layer capacitance, R is the overall device differential resistance, L is due to space charge effects and R_s is the parasitic series resistance.

device	area (μm^2)	bias (V)	R (Ω)	L (nH)	C (pF)	R_s (Ω)
A	52	0.5	653	3.1	0.1	63.7
		2.0	118	0.3	0.1	64
B	52	2.0	2300	5.0	0.005	65
C	225	2.0	413	1.23	0.12	20.7

Table 2.1 Values of the equivalent circuit elements determined from small signal impedance measurement.

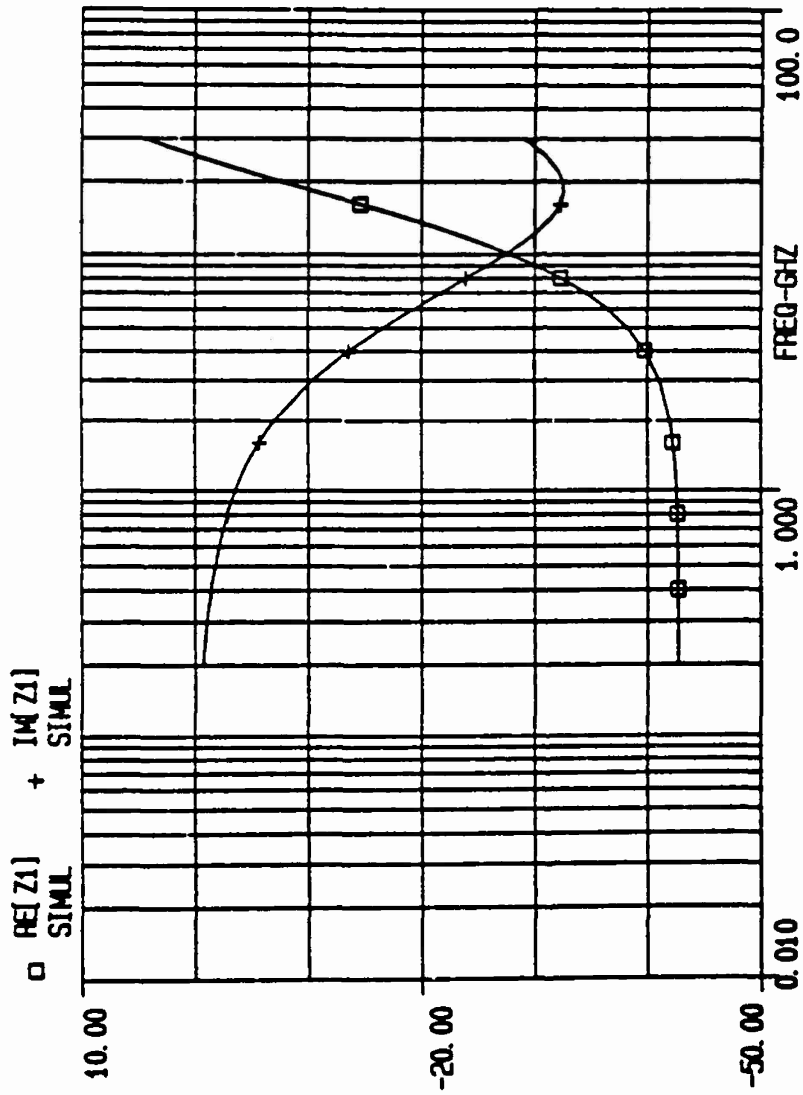


Fig. 2.12 Small signal impedance of the device C in the negative resistance region

that the same device can maintain its negative resistance well above 100 GHz.

2.5-Discussion and Conclusion

Using small signal analysis of the QWITT diode and the slope of its DC I-V curve, the microwave impedance of the device can be calculated. The calculated values of the impedance are in close agreement with experimental measurements. The theoretical model uses only the DC I-V characteristics of the QWITT diode as well as information about the device structure and the parasitic series resistance to predict its impedance. Thus, it was confirmed that the small signal RF behavior of QWITT diodes is well predicted by the small signal model, which can then be used to determine the optimum device structure necessary to maximize its negative resistance.

The series resistance due to ohmic contacts for several QWITT diodes was determined. Due to the large series resistance ($10^{-5} \Omega \text{ cm}^2$) of the QWITT diodes that were tested, one can not expect oscillation frequencies higher than 30 to 40 GHz.

CHAPTER 3

QWITT DIODE OSCILLATORS

SMALL SIGNAL ANALYSIS AND DESIGN

An oscillator relies on device nonlinearity for operation and is inherently a nonlinear system. Due to nonlinear operation, higher-order harmonics are generated that affect the frequency of oscillation, the power generated and the efficiency of the oscillator. It is only by nonlinear analysis that one can determine the exact frequency of operation, the power and efficiency of the oscillator, and the power generated at higher harmonics relative to the power generated at the fundamental frequency. However, based on some simplifying assumptions, we can perform a small signal analysis of an oscillator. By using the small signal analysis, we can design the oscillator circuit and optimize its performance.

In this chapter, some basic concepts concerning the small signal analysis of negative resistance oscillators are described. Also, a procedure for small signal analysis is explained which makes the oscillator design using existing computer aided design tools easier. Then three types of planar QWITT diode oscillators designed using the small signal analysis are presented.

3.1-Negative Resistance Oscillator Design

The basic analysis of microwave negative resistance oscillators is explained by Kurokawa [9]. A microwave oscillator is shown in Fig. 3.1. The circuit consists of a nonlinear negative resistance device and a resonance circuit. The impedance of the circuit as a function of frequency is expressed by $Z(\omega)$. The impedance of the device in

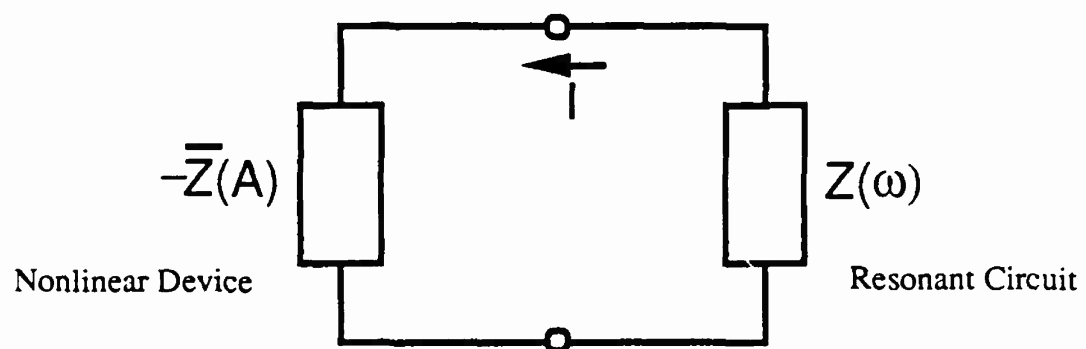


Fig. 3.1 Equivalent circuit of a free-running microwave oscillator

general is a function of frequency as well as the amplitude of the ac voltage or current across or through it. In the following discussion, we assume that the impedance of the device is only a function of the amplitude of the ac signal and it is expressed by $Z(A)$. This assumption is usually justifiable since the device impedance is a slowly varying function of the frequency compared to the circuit impedance $Z(\omega)$. We assume the current

$$i(t) = \text{Re}[Ae^{j(\omega t + \phi)}] + (\text{small harmonic components}) \quad (3.1)$$

is flowing in the circuit. We can determine the voltage across the device and the resonant circuit. Depending on the device and circuit impedances, the harmonic voltages across them may not be negligible. For free running oscillators, the sum of the voltages across the device and the circuit must be equal to zero since no external voltage is applied. By applying orthogonality between trigonometric functions and some algebra, we can obtain the steady state condition for oscillation which is given by:

$$Z(\omega) = -Z(A) \quad (3.2)$$

where

$$Z(\omega) = R(\omega) + jX(\omega) \quad \text{and} \quad Z(A) = R(A) + jX(A) \quad (3.3)$$

The oscillation frequency and amplitude are determined by plotting the locus of the circuit impedance (called the impedance line) and the locus of the negative of the device impedance (called the device line) on the complex impedance plane (Fig. 3.2). The point which the device line and the impedance line intersect determines the steady state operating point and the amplitude and the frequency of the oscillation can be

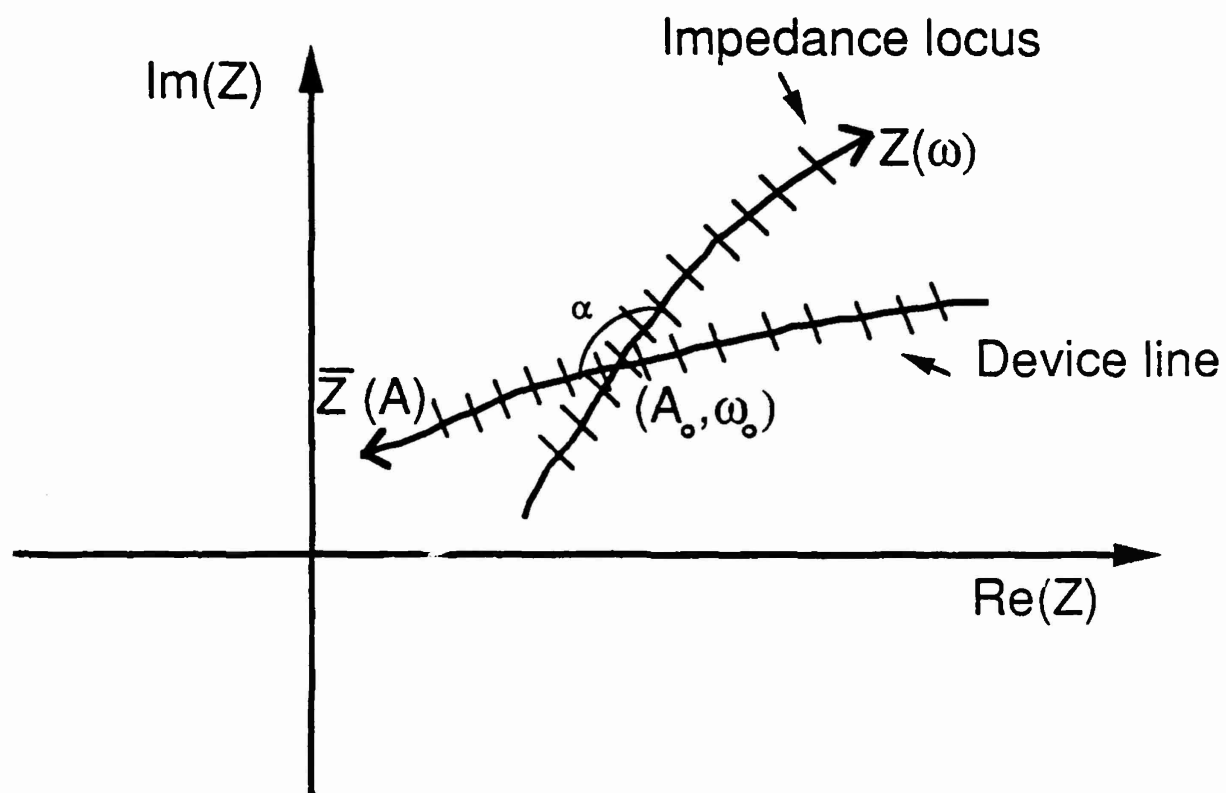


Fig. 3.2 Impedance locus and device line. The operating point is the point of intersection.

determined. Also Kurokawa derives the condition for the stability of the operating point. The intersecting angle measured clockwise from the device line in direction of increasing A (see Fig. 3.2) to the impedance line in direction of increasing ω must be less than 180° for the operating point to be stable.

Even though the steady state oscillation condition always holds, often there is a difficulty in determining the operating point as it was discussed above. This is because determining the impedance of the device as a function of the amplitude of voltage across it requires a nonlinear model for the device which is not simple and may not be available. The first order one port negative resistance oscillator analysis can also be performed by an alternate approach utilizing the traveling wave concept and employing a reflection coefficient description of the active device and circuit elements [10]. Consider a one port active circuit with S parameter S_{11} connected to a resonant load with reflection coefficient Γ (Fig. 3.3). Note that both S_{11} and Γ are measured at the same reference plane. Suppose a noise signal E is incident on the active circuit port. The reflected signal from the active circuit is $S_{11}E$. This signal is incident on the port of the resonant load and re-reflected back. The re-reflected signal from the resonant load is given by $S_{11}E\Gamma$ which will again be incident on the input of the active device. These reflections add up to give an infinite series. The steady state condition for oscillation is given by:

$$S_{11}\Gamma = 1 \quad (3.4)$$

This approach is more compatible with computer aided microwave circuit design because all the information is generally expressed in terms of reflection coefficients.

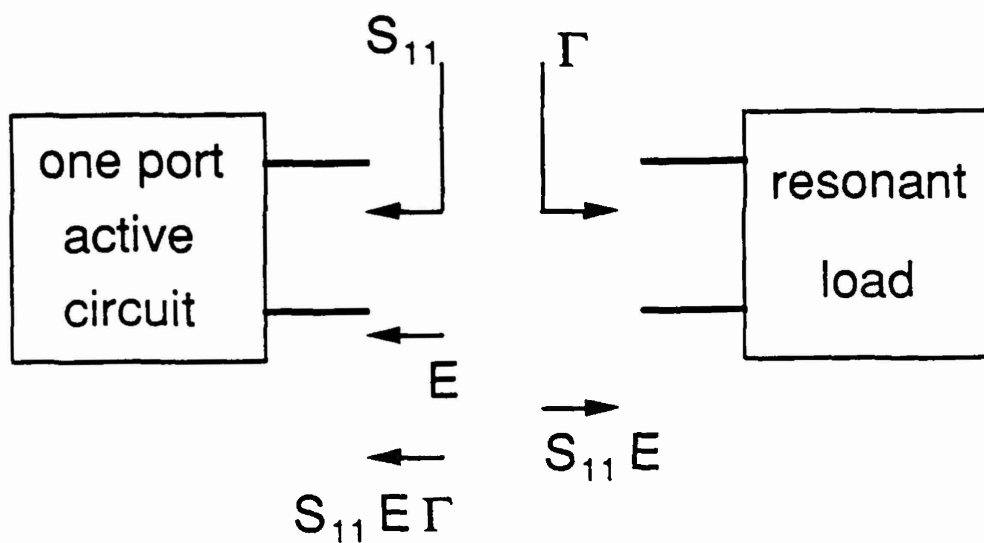


Fig. 3.3 An oscillator as a reflection amplifier

In general in oscillator design we are not as much interested in knowing the exact amplitude of the oscillation as maximizing the output power by proper circuit design. Also we often have only information about the small signal behavior of the negative resistance device. Therefore by using some simplifying assumptions we can perform the oscillator design based on the small signal model for the negative resistance element.

As a first approximation we assume the frequency dependence of the negative resistance device can be neglected. As it was mentioned this is valid only for a small range of frequencies depending on the type of the negative resistance device. In the range of the frequencies where the above assumption is valid, the negative resistance device may be characterized by a cubic function relating instantaneous current to instantaneous voltage across the device. This relation is given by

$$I = a_1 V + a_2 V^2 + a_3 V^3 \quad (3.5)$$

For a negative resistance device a_1 is a negative number. The effect of the term $a_2 V^2$ is to shift the I-V characteristic to an unsymmetric point. For analysis of fundamental mode oscillation we set the quadratic term to zero. This type of I-V characteristic was first used by Van der Pol (where $a_2 = 0$) in his classic work on nonlinear oscillators [11]. It should be mentioned that this approximation is not a static property of the active device (it need not be valid for DC), but it means that the device at a certain frequency presents negative resistance and can generate oscillations which are limited in amplitude. Even though this model is used to describe the dynamic behavior of devices

like Gunn diodes and MESFETs, it is even more realistic for tunnel, quantum well and QWITT diodes since these elements exhibit static characteristics (DC I-V curves) very similar to the one described by Eq. 3.5. The value of a_1 is taken as the small signal negative conductance of the device and a_3 is chosen such that the highest generated power should be equal to the highest available power of the diode [12]. The dynamic conductance of the device is determined by differentiating Eq. 3.5; which gives:

$$G = a_1 + 3a_3V^2 \quad (3.6)$$

In the above equation, we define the small signal conductance G_0 of the negative resistance device as $G_0 = a_1$. We can assume a voltage $V = \sqrt{2}V_0\cos \omega t$ appears across the device terminals. This is based on the assumption that all the higher harmonics are negligible. The power generated can be calculated as the period average of the voltage-current product. Based on the expression for the power we can define an RMS negative conductance for the device [12]. After satisfying the condition for steady state oscillation and maximizing the power expression, we can determine the condition for maximum power generation relating the load conductance G_L to the small signal negative conductance of the device G_0 . This condition is given by

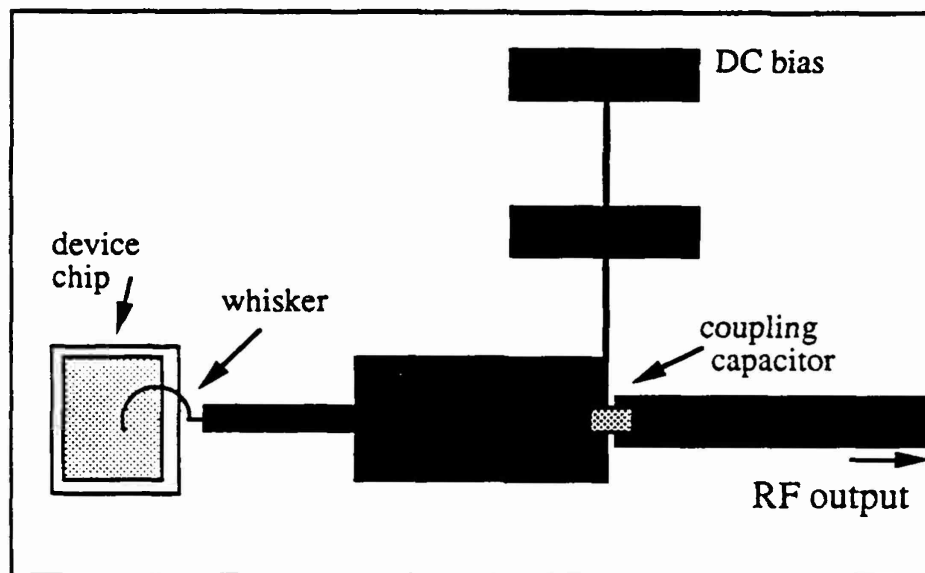
$$G_L = \frac{1}{2} |G_d| \quad (3.7)$$

which means highest power is obtained when the load conductance is equal to half of the small signal negative conductance of the device. Of course at the oscillation frequency the sum of the imaginary parts of the circuit and the device impedance should be zero.

3.2-Design of Planar QWITT Diode Oscillators

Based on the discussions in Chapter 3.1 and using the small signal impedance of the QWITT diode obtained from the theoretical model (explained in Section 2.1), several planar QWITT diode oscillators were designed. The microwave circuit design was performed based on the small signal oscillator circuit design and by using Touchstone™ microwave CAD program available from EEsof Corporation of Westlake Village, CA.

A planar QWITT diode oscillator is shown in Fig. 3.4. The circuit is fabricated on a woven Teflon™ substrate with a dielectric constant of 2.5. The substrate thickness is 32 mils. The chip containing QWITT diodes is contacted to the ground plane of the substrate by using silver paint. A single QWITT diode is connected to the microstrip line circuit through a whisker contact. The whisker is made of gold-plated phosphor-bronze and has a diameter of 0.5 mil. The whisker is modeled as a small inductor in series with the device. The whisker is connected to a microstrip line which moves the impedance of the QWITT and that of the whisker to a point on the real axis of the Smith chart. The second piece of the microstrip line is a quarter wave transformer which matches this point to a resistive load for maximum power generation. The entire circuit can act as a parallel resonant structure. Since the structure is parallel resonant, the condition for start up oscillation is satisfied when the small signal negative conductance of the device is larger than the load conductance and the condition for the maximum power transfer is that the conductance of the load should be half of the small signal negative conductance of the diode ($G_L = 1/2|G_0$). The



ER = 2.55 H = 33 mils T = 1.4 mils

Fig. 3.4 A planar QWITT diode oscillator

microstrip line structure is connected through a DC blocking capacitor to an SMA connector. The structure is biased through a bias filter.

A very important part of the QWITT diode oscillator design is the biasing scheme. Since the device maintains its negative resistance from DC to microwave frequencies, parasitic oscillations can occur at any point where there is a resonance in the bias line. Since, in general, the Q of a resonant structure is higher at lower frequencies, the circuit has a tendency to oscillate at lower resonance frequencies rather than at the desirable frequency of oscillation. Therefore, in order to prevent any bias line oscillation, the biasing structure should be made very lossy. This can be done by loading the bias line structure using resistive elements. Some by-pass capacitors can also be used to short out the parasitic oscillations at lower frequencies.

Fig. 3.5 shows another type of planar QWITT diode oscillator. A QWITT diode is connected to a half-wave microstrip resonator via a whisker contact. The frequency of oscillation is basically determined by the half-wave resonator. The output of the structure is connected through a bias tee to a triple stub tuner. The function of the stub tuner is to maximize the power generated from the device by matching the device impedance to 50 ohms.

3.3-Experimental Results for Planar QWITT Diode Oscillators

The heterostructures used in this study were grown in a Varian GEN II MBE system on n^+ GaAs substrates. A schematic diagram of the device structures used is shown in Fig. 3.6. Three QWITT device structures, A, B and C, consisting of identical quantum well regions but with three different n^- GaAs drift regions lengths of

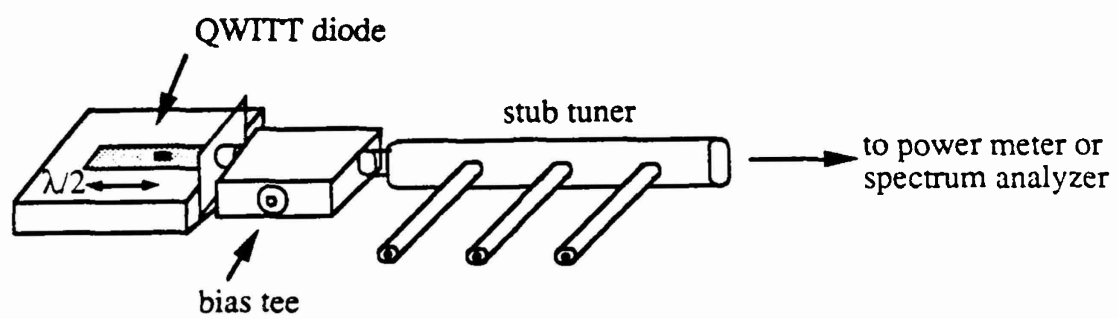


Fig. 3.5 A planar QWITT diode oscillator using a microstrip half wave resonator

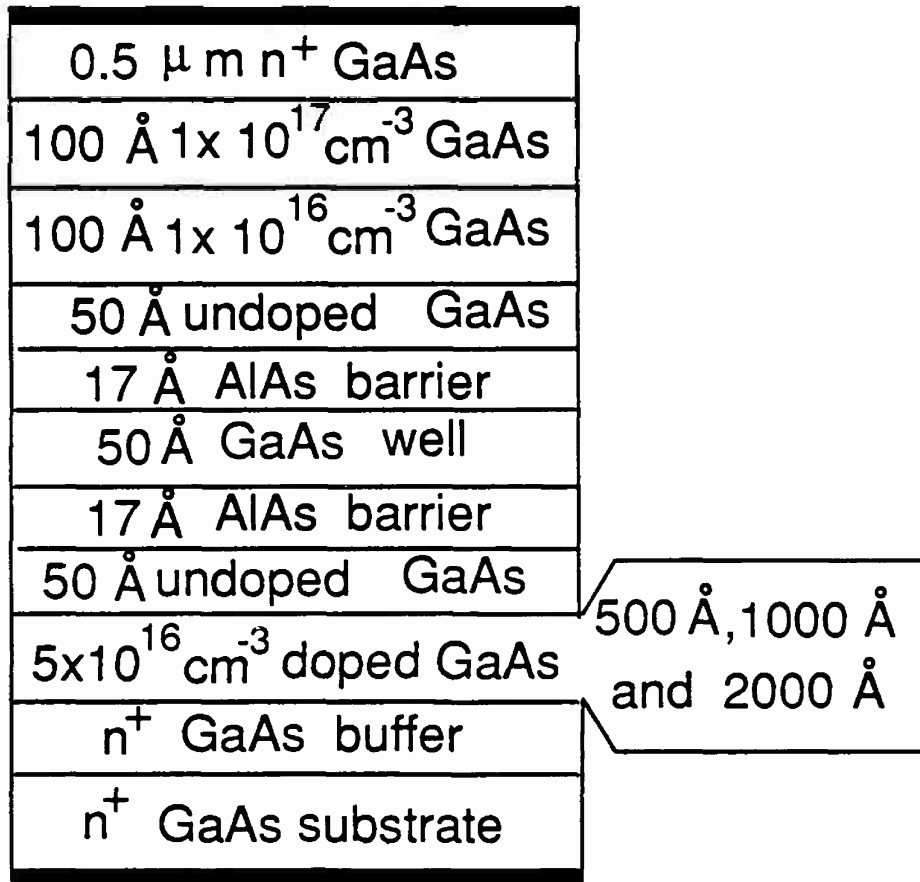


Fig. 3.6 Cross section of the QWITT diode structures A, B and C

500, 1000 and 2000 Å, respectively, were examined [13]. A maximum depletion region length of 2000 Å was chosen, since that corresponds to the optimum length of the drift region for 10 GHz operation based on the small signal model for the QWITT diode [7]. The quantum well regions consisted of a 50 Å GaAs layer sandwiched between two AlAs layers 17 Å thick. The AlAs barrier layers were kept thin to increase the current density through the device. Device diameters were typically 4-8 μm, corresponding to a device area of $1.25-5 \times 10^{-7} \text{ cm}^2$. Continuous and pulsed DC current-voltage characteristics at room temperature were measured. The room temperature DC I-V curves of devices A and C are shown in Fig. 3.7. Based on the I-V curve and device structures, the small signal impedances of the devices were calculated.

For QWITT devices containing a uniformly doped depletion region, the large signal model [8] indicates that the electric field in this region is of the order of 100 kV/cm. For GaAs, electric fields around 3-10 kV/cm are sufficient to have carrier velocities around 10^7 cm/s . Hence, a doping spike at the beginning of the drift region could be introduced so that the electric field in the GaAs drift region is reduced, and yet the entire drift region is fully depleted. This should result in a reduction in the DC bias across the device and hence improve the DC-to-RF conversion efficiency. Since the entire drift region is still depleted, the voltage swing between peak and valley would remain the same. Fig. 3.8 shows the schematic of the device structures, D through G, examined in this study. The room temperature DC I-V curves for devices D and E are shown in Fig. 3.9.

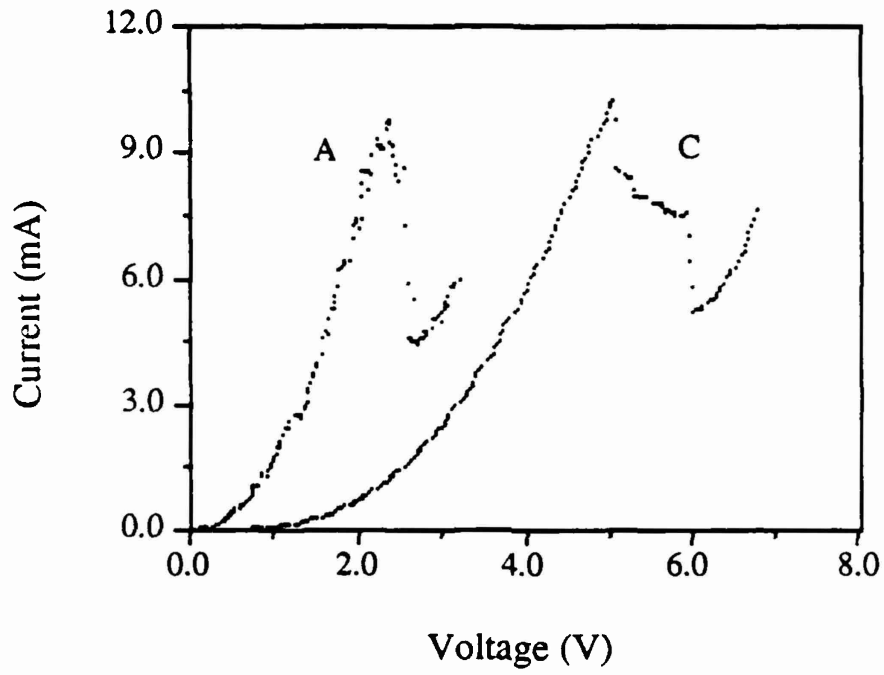


Fig. 3.7 Room-temperature DC I-V curves for QWITT devices A and C with 500 Å and 2000 Å depletion region lengths respectively.

0.5 μm n^+ GaAs	
100 \AA $1 \times 10^{17} \text{cm}^{-3}$ GaAs	
100 \AA $1 \times 10^{16} \text{cm}^{-3}$ GaAs	
50 \AA undoped GaAs	
17 \AA AlAs barrier	
50 \AA GaAs well	
17 \AA AlAs barrier	
150 \AA undoped GaAs	
100 \AA GaAs spike	← Doping spike
1800 \AA	
$5 \times 10^{16} \text{cm}^{-3}$ doped GaAs	
n^+ GaAs buffer	
n^+ GaAs substrate	

Fig. 3.8 Cross section of the QWITT diode structures with a doping spike, D through through G.

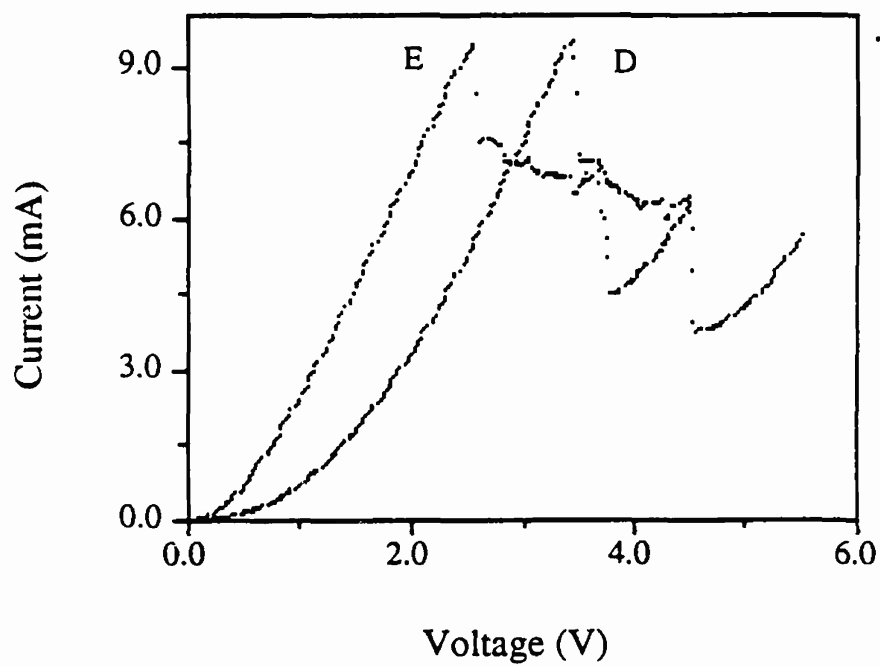


Fig. 3.9 Room temperature DC I-V curves for QWITT devices D and E with a Si doping spike of $5 \times 10^{16} \text{ cm}^{-3}$ and $1 \times 10^{17} \text{ cm}^{-3}$, respectively.

The microwave performance of different QWITT diode structures, A through G is summarized in tables 3.I and 3.II. From the first planar structure described in Section 3.2, a maximum power of 1 mW was obtained [14]. This corresponds to an output power density of 3.5-5.0 kW/cm² for a device area of 2-3.5x10⁻⁷ cm² (5-6 μm in diameter). This result is the highest output power obtained from any quantum well oscillator at any frequency and shows approximately five times higher power and two to three times higher output power density than reported in the literature [15] for a comparable frequency. These results also represent the first planar circuit implementation of a quantum well oscillator.

In devices D through G (see Fig. 3.7) a doping spike was introduced at the beginning of the drift region to reduce the electric field and thus decrease the DC bias voltage. By optimizing the doping concentration of the doping spike, an increase in efficiency from 3 to 5 percent has been obtained, without compromising the output power at X-band. It is clear that there is considerable room for optimization of both the device and circuit, to maximize RF output.

The planar circuit shown in Fig. 3.5 was also tried. By adjusting the size of the half-wave resonator the frequency of the oscillation was adjusted, and the output power was maximized by adjusting the stub tuner. At 15 GHz, the maximum power was -6 dBm and at 19 GHz, the maximum power was approximately -12.8 dBm. Compared to results of harmonic balance analysis of a QWITT diode oscillator [16], the power levels that we have obtained so far are much smaller than predicted values. Part of the problem is caused by the large series resistance of our QWITT devices due to the

Length of Drift Region (Å)	Specific Negative Resistance (10^{-5} Ohm-cm ²)	Output Power (mW)	Oscillation Frequency (GHz)
500	2.6	240	10.0
2000	6.8	275	6-8

Table 3.1 Results obtained from planar QWITT diode oscillators

Doping Spike (cm^{-3})	Output Power (μW)	Efficiency	Oscillation Frequency (GHz)
5×10^{16} (D)	850	3.5%	5-8
8×10^{16} (E)	1000	5.0%	5-8
1×10^{17} (F)	350	4.3%	5-8
5×10^{17} (G)	100	3%	5-8

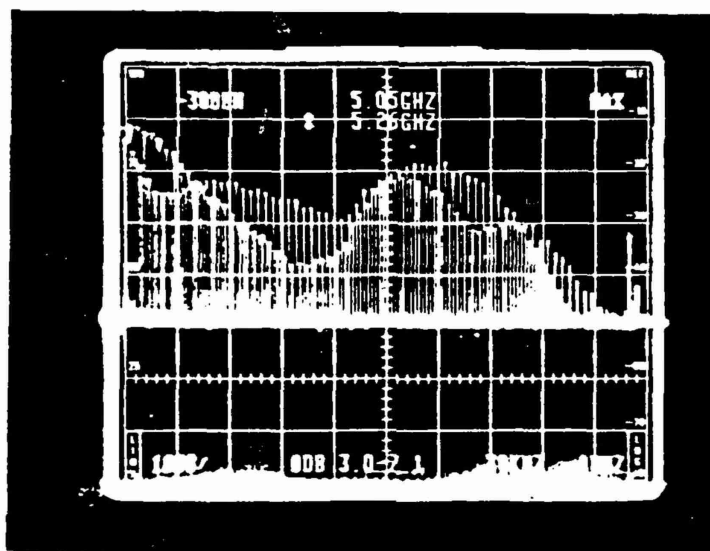
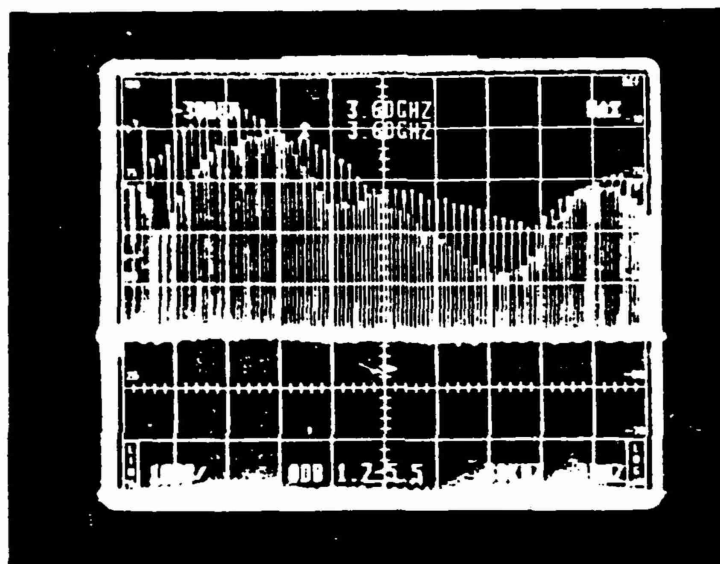
Table 3.11 Microwave performance of QWITT diode oscillators D through G in planar microstrip circuits

ohmic contacts (as was mentioned in Chapter 2, the series resistance for diodes with an area of about $50 \mu\text{m}^2$ is 60 ohms.).

In some cases when the bias line oscillation was not prevented, low frequency oscillations (as low as several MHz) were observed. Due to the nonlinearity of the device, higher order harmonics were also generated. For example, in one case, as shown in Figs. 3.10a and 3.10b, the fundamental frequency of oscillation was 30 MHz. Higher order harmonics up to 7 GHz were detected using a spectrum analyzer. As shown in the photograph taken from the spectrum analyzer's screen, more than 200 spectral lines are present. The separation between each two of them is 30 MHz (Fig. 3.11). Based on these observations, it seems that the QWITT diode has a potential to be used as a very broad band microwave comb generator. It seems that the higher harmonics generated are not merely due to the nonlinearity of the device, because if this was the case the power of the harmonics would be roughly proportional to the inverse square of frequency. Besides the nonlinearity of device itself, another reason for a large harmonic content is relaxation type oscillations.

3.4-Attempts to Design a 94 GHz QWITT Diode Oscillator

A planar QWITT diode oscillator at 94 GHz was also designed. The planar circuit is shown in Fig. 3.12a. A QWITT diode is whisker contacted to a half-wave microstrip resonator which determines the frequency of oscillation. The device is biased through a low-pass filter. The structure is connected to an antipodal finline transition through a wide band DC block. The function of the finline transition is to convert energy from the microstrip mode to the waveguide mode. The planar structure is inserted in the E-plane of a W-band waveguide (Fig. 3.12b). Unfortunately, as we



Figs. 3.10a and 3.10b Spectrum analyzer display of a QWITT diode relaxation oscillator

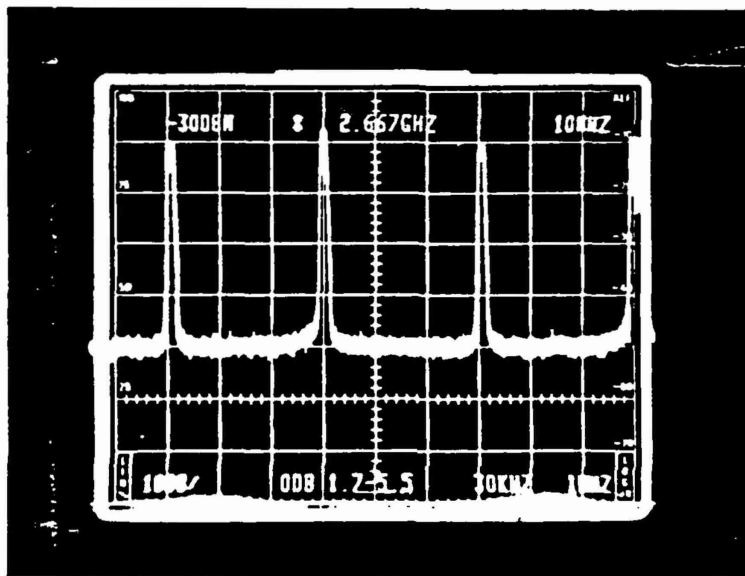


Fig. 3.11 Zoomed display, harmonics are separated by 30 MHz

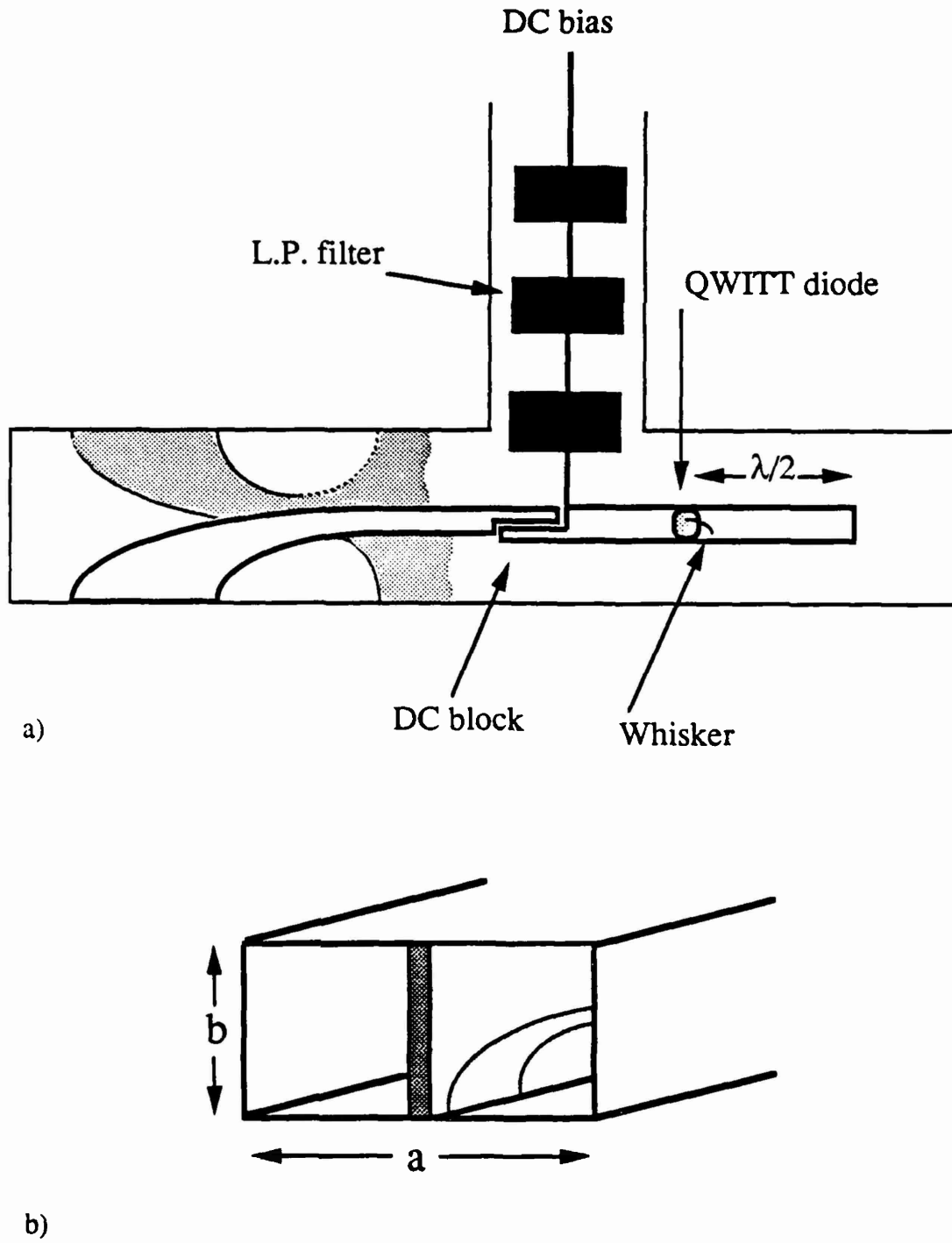


Fig. 3.12 a) A planar W-band QWITT diode oscillator
 b) The structure is inserted in the E-plane of a W-band waveguide

expected, mainly due to the large parasitic series resistance of the QWITT diodes (Chapter 2), no oscillation around 94 GHz was detected. The structure oscillated at about 5 GHz which could be detected through the bias line. This parasitic oscillation could have been due to a resonance in the bias line or due to the parasitics introduced by the whisker contact.

3.5-Conclusion

In this chapter, experimental results obtained from several QWITT diode oscillators were presented. A peak output power of 1 mW, corresponding to an output power density of 3.5-5 kW/cm², in the frequency range of 5-8 GHz has been obtained. This is the highest output power obtained from any quantum well oscillator at any frequency and provides approximately five times higher power and two to three times higher output power density than reported in the literature for a comparable frequency. This result also represents the first planar circuit implementation of a quantum well oscillator.

CHAPTER 4

SELF OSCILLATING QWITT DIODE MIXERS

In the I-V curve's negative resistance region, the quantum well and the QWITT diode's dynamic conductances are strong functions of the AC signal across them. Therefore, quantum well and QWITT diodes are expected to be useful as good performance mixers. Ordinary mixers using nonlinear devices like Schottky diodes have some conversion loss. Devices like quantum wells and QWITT diodes are nonlinear negative resistance elements and can be used as self oscillating mixers. Due to the presence of negative resistance, self oscillating mixers are expected to have some conversion gain.

In this chapter experimental results using the QWITT diode as an X-band self oscillating mixer operating in both waveguide and planar circuits are presented. The waveguide mixer operates in the third harmonic conversion mode while the planar mixer operates as a fundamental mode mixer. The waveguide mixer circuit can either be tuned to have a narrow intermediate frequency (IF) bandwidth with a conversion gain of about 10 dB or to have a broad IF bandwidth with a conversion loss of about 4 dB. The planar mixer exhibits a narrow-band conversion gain of 4 dB or a broad-band conversion loss of 8 dB. These are the first experimental results showing conversion gain from a self oscillating mixer using a quantum well diode.

4.1-Basic Mixer Theory

To simplify the problem, it is assumed that mixing is caused only by a nonlinear resistor. For small signal analysis, it is assumed that the local oscillator (LO) power is

much larger than the RF power injected into the resistive mixer. Therefore, the dynamic conductance of the device can be determined by analyzing the interaction between LO signal and the diode. The device nonlinear I-V characteristic is represented as a relationship between the current and voltage:

$$i = f(v) \quad (4.1)$$

Due to device nonlinearity, the LO voltage across the diode is not sinusoidal. The LO signal can be represented by its Fourier series as:

$$v(t) = \sum_{m=-\infty}^{+\infty} v_m e^{jm\omega_0 t} \quad (4.2)$$

where ω_0 is the fundamental LO frequency. The values of v_m are obtained by performing a nonlinear analysis. We can determine the time dependent conductance of the device, $g(t)$, resulting from the mixer being pumped by the LO signal. $g(t)$ can be represented by its Fourier series:

$$g(t) = \left(\frac{di}{dv} \right)_{v(t)} = \left(\frac{df(v)}{dv} \right)_{v(t)} = \sum_{n=-\infty}^{+\infty} g_n e^{jn\omega_0 t} \quad (4.3)$$

If a RF signal with a small amplitude v_s and frequency ω_s is applied across the diode we can determine the output current:

$$i(t) = g(t)v_s e^{j\omega_s t} = \sum_{n=-\infty}^{+\infty} g_n v_s e^{j(n\omega_0 + \omega_s)t} \quad (4.4)$$

Ordinarily the $-\omega_0 + \omega_s$ term is filtered out for use as the intermediate frequency (IF). From Eq. 4.4 the conversion loss of the mixer can be determined. The above analysis can also be applied to self-oscillating mixers since it only requires the actual LO voltage across the device.

Also, by considering the dynamic I-V characteristic of the QWITT diode, one can conclude the following statements. If the diode is biased in the middle of the negative resistance region where the I-V curve is antisymmetric, the diode's dynamic conductance can be represented by a second order polynomial. The Fourier series of the time varying conductance has large components at the even harmonics of the oscillation frequency. In this case, the self oscillating QWITT diode mixer has its highest conversion efficiency in the second harmonic mode of operation. The fundamental mode of mixing will have its highest efficiency when the device is biased at the point where the I-V curve has its highest curvature [15].

4.2-Experimental Results and Discussion

A schematic diagram of the QWITT diode structures examined in this study is shown in Fig. 3.6. In the waveguide circuit the QWITT diode is mounted on a micrometer controlled post which is in electrical contact with the waveguide walls. The DC bias is provided using a whisker contact which is connected to a metallic post inside the waveguide. An E/H plane tuner is used to minimize RF reflection and improve the conversion efficiency. The sliding short in the waveguide can also be adjusted to improve the conversion efficiency. The waveguide circuit operated as a harmonic mixer, since the fundamental frequency of oscillation of the QWITT was about 3 GHz,

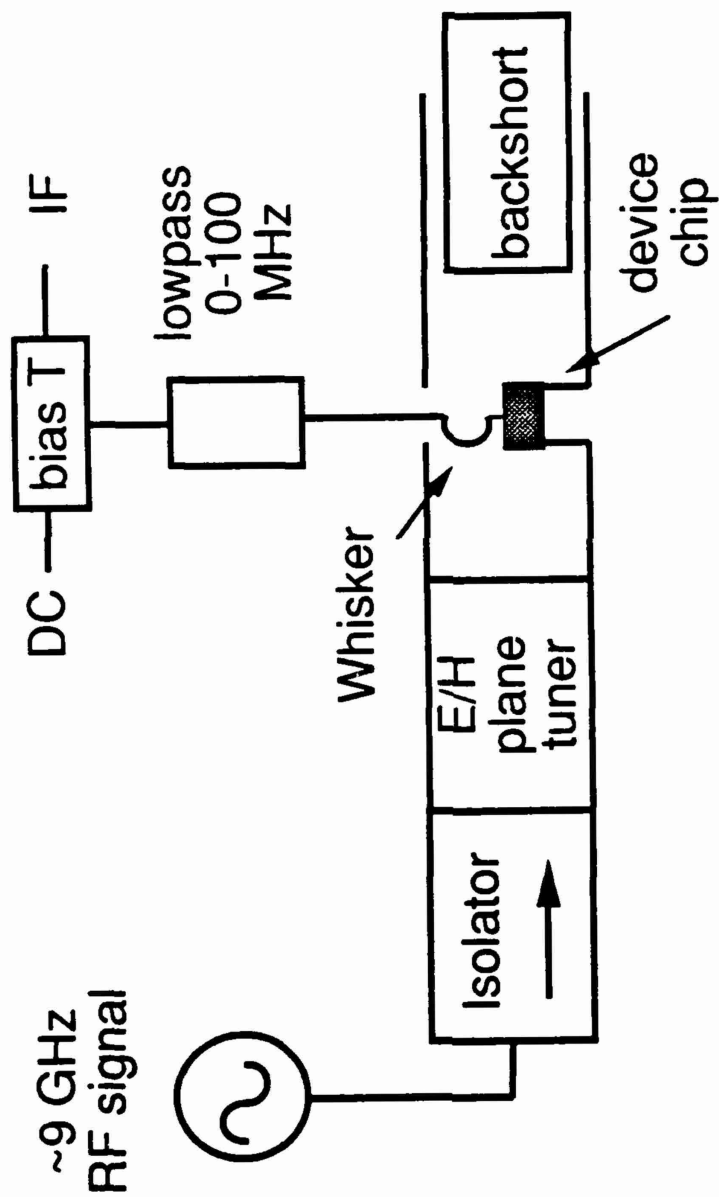


Fig. 4.1 Block diagram of waveguide self-oscillating harmonic mixer. A fundamental oscillation at about 3 GHz acted as a harmonic LO for mixing with a 10 GHz RF signal.

due to a resonance in the bias line circuit. A schematic diagram of the waveguide harmonic mixer is shown in Fig 4.1. The RF source is isolated from the self-oscillating mixer circuit using an isolator. The isolator is used to prevent the LO signal from going into the RF source. The RF signal is mixed down with the third harmonic of the LO. The IF signal is monitored through a low-pass filter and bias tee external to the waveguide mount. The low-pass filter is used to prevent any high frequency components from reaching the IF line. The bias line resonance was primarily due to parasitics in the whisker mount, since the external filter and bias tee network had very little influence on the fundamental oscillation of the QWITT diode. In addition, since the fundamental frequency is below the waveguide's cut off frequency, the effect of the E/H plane tuner and the back short on the oscillation was slight.

By adjusting the E/H plane tuner, the back short, and the bias voltage, 5 to 12 dB of conversion gain with an IF bandwidth of 10-20 MHz has been achieved. This conversion gain can be obtained over RF frequencies between 8 and 10 GHz by retuning the back short, the E/H plane tuner and the bias voltage. The IF frequencies can be in the range approximately from 50 MHz to 1 GHz (see Fig. 4.2). The LO frequency also varies with DC bias voltage, which is reflected in the changes of the IF.

Broad-band operation (IF bandwidth greater than 100 MHz) is also achievable by tuning the mixer as mentioned above. In this mode of operation, conversion loss of about 5 ± 2 dB is observed over the entire IF bandwidth (Fig. 4.3). In all the above cases, the RF power injected is about -55 dBm and the power at the third harmonic of the fundamental QWITT oscillation is about -15 dBm. Devices with different drift

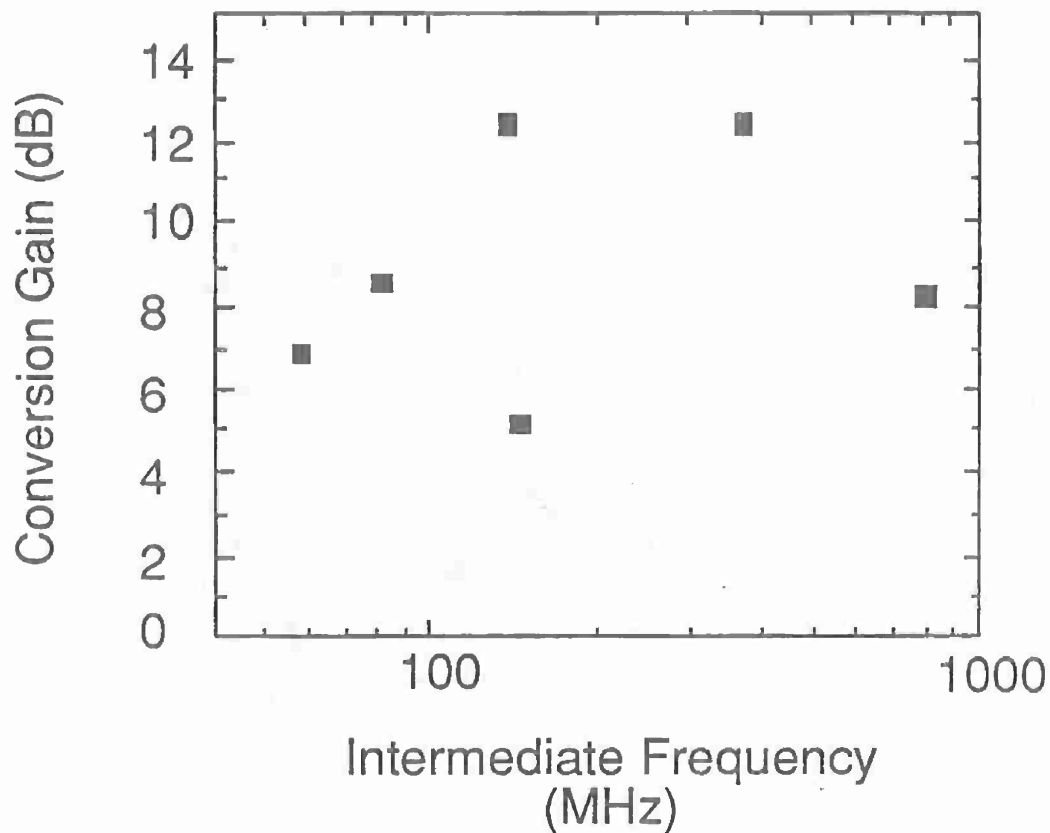


Fig. 4.2 Conversion gain as a function of intermediate frequency for the X-band waveguide harmonic mixer using a QWITT diode with a 2000\AA depletion region. For each new IF the system was retuned to obtain maximum conversion efficiency; at a fixed IF, the bandwidth was only about 20 MHz.

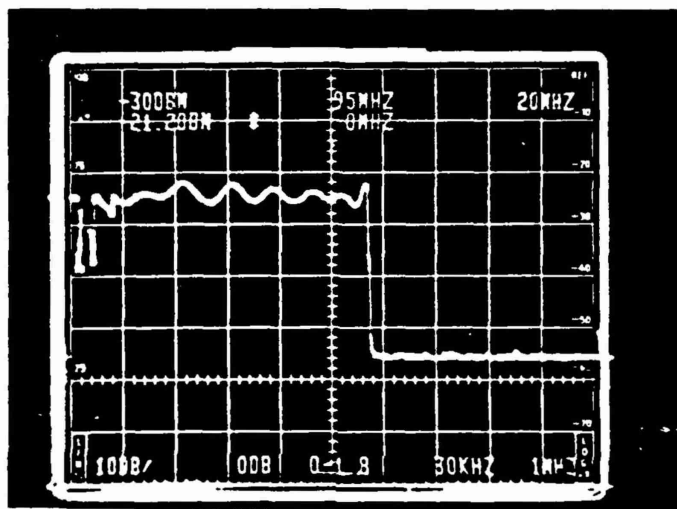


Fig. 4.3 Photograph of broadband IF signal. The spectrum analyzer screen is set to storage mode. The IF variation is between 2 to 100 MHz and its power fluctuation is about ± 2 dB. The RF power injected was -49 dBm centered at 9.3 GHz.

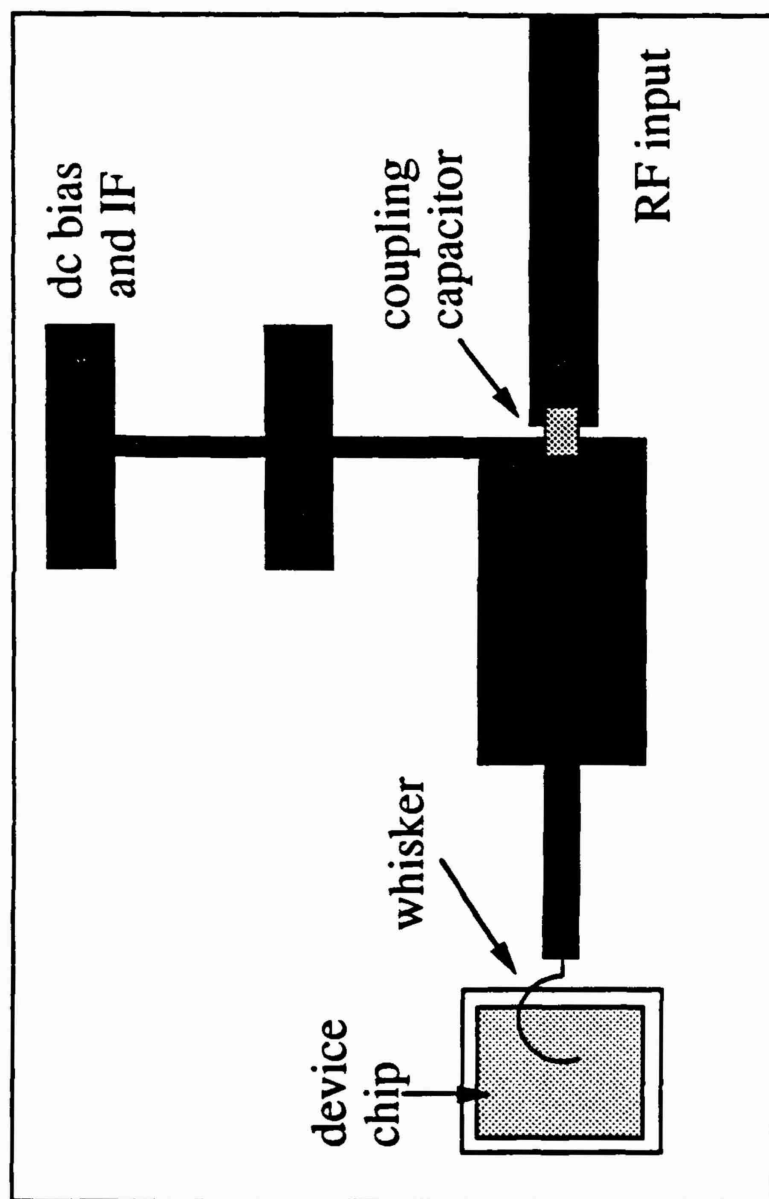


Fig. 4.4 Diagram of a microstrip planar self-oscillating mixer circuit; this circuit operated in the fundamental mode. No external tuning elements were used with the planar circuit.

region lengths from 500 Å to 2000 Å have been examined; conversion gain has been obtained only from the 2000 Å drift region device.

The planar self oscillating mixer uses a microstrip resonant circuit (Fig. 4.4), identical to that used for the oscillator experiments [17], and operates in the fundamental conversion mode. No external tuning elements were used with this circuit. Here the fundamental oscillation frequency of the QWITT is about 10 GHz. The author was able to obtain conversion gains of about 4 dB over a narrow bandwidth of 10-20 MHz, where only the DC bias was varied to maximize conversion efficiency. For other DC biases, larger bandwidths (40-200 MHz) could be obtained with conversion loss of about 10 ± 1.5 dB over the entire band. The RF power injected here was about -45 dBm and LO power was about -3 dBm.

Using a spectrum analyzer for absolute power measurement and assuming that the spectrum analyzer itself does not contribute to noise, an attempt was made to estimate an upper bound for the noise figure of the self oscillating mixer. The noise figure of the waveguide mixer, at an IF frequency of 100 MHz where conversion gain was about 8.6 dB, was estimated to be about 15.5 dB (corresponding to a noise temperature of about 9710 °K).

4.3-Conclusion

It was demonstrated that self oscillating QWITT diode mixers have the ability to produce conversion gain at X-band. The waveguide mixer exhibits a conversion gain of about 10 dB in a narrow bandwidth, and a conversion loss of about 5 dB if broadband operation is desired. The planar mixer circuit exhibits a narrow-band conversion

gain of 4 dB or a broad-band conversion loss of 10 dB. As was mentioned, the highest efficiency from a quantum well mixer is obtained (if it is biased in the middle of the negative resistance region) when it operates in second harmonic conversion mode. Therefore, there is considerable room for optimization in both device and circuit design and it is conceivable that even better RF performance may be obtained in the future.

CHAPTER 5

A PERIODIC POWER COMBINING STRUCTURE

The power produced from millimeter wave sources drops drastically as their frequency of operation increases. In spite of the fact that devices like resonant tunneling diodes maintain their negative resistance up to THz, they are very low power devices. This was indeed the motivation behind the introduction of QWITT diode. When the QWITT is compared to devices like the IMPATT, the power it generates is still small, even though the QWITT diode has the potential to operate at higher frequencies. Based on the above discussion, there is a strong need for techniques to combine power from several millimeter wave generators to achieve higher powers.

There has been extensive research conducted in the area of power combining techniques. A summary of different techniques is given by Chang and Sun [18]. Classical power combining techniques were developed in waveguide cavities [19]. These types of power combining structures are not very useful in the millimeter wave region due to the fact that the dimensions of the waveguide cavity become very small and therefore the number of devices that can be power combined is limited. Also these types of power combining structures are very bulky when compared to the planar structures and therefore are not suited for space applications. It is desirable to design a simple planar power combining oscillator convenient for monolithic fabrication. One way to achieve this goal is through distributed oscillators which allow power combining of several negative resistance devices [20, 21]. In this method, negative resistance devices are inserted periodically one half wavelength apart in a planar transmission line structure like parallel plate waveguide or microstrip line. This makes

the use of external resonator circuits unnecessary and the design of monolithic circuit easier. In order to demonstrate this method several Gunn devices were used, because Gunn diodes are available in package form and are well characterized. The results of several distributed power combining Gunn diode oscillators are presented here. In some of the cases, power combining efficiencies larger than 100% are obtained.

5.1-Theory

A distributed power combining oscillator is shown in Fig. 5.1. A transmission line with the characteristic admittance Y_0 is loaded periodically with admittances Y_p each separated by a distance "d". The admittance Y_p is the sum of the admittance of the active device and all the parasitics due to discontinuities. Using a simple admittance transformation, we can calculate the admittance Y_{in} as a function of frequency [22]. The frequency at which the imaginary part of the Y_{in} goes to zero is the resonance frequency of the structure (Fig. 5.2). To satisfy the oscillation condition, the value of the termination conductance G_L should be equal to $-\text{Real}(Y_{in})$ at the resonance frequency. If Y_p contains only a real part, the periodicity of the structure will be equal to a half wavelength at the oscillation frequency ($d = \lambda/2$). Since in this case the diodes are separated by a half wavelength, they are effectively in parallel. Therefore, all of them see the same impedance and operate at the same operating point. To counter-balance the reactive part of the admittances Y_p , several shunt inductive stubs can be used (it is assumed that the reactive component of the admittance is capacitive) (Fig. 5.3). The shunt inductive stubs compensate the reactive component of the diodes' impedance at the oscillation frequency. Of course, a single stub at the end of the

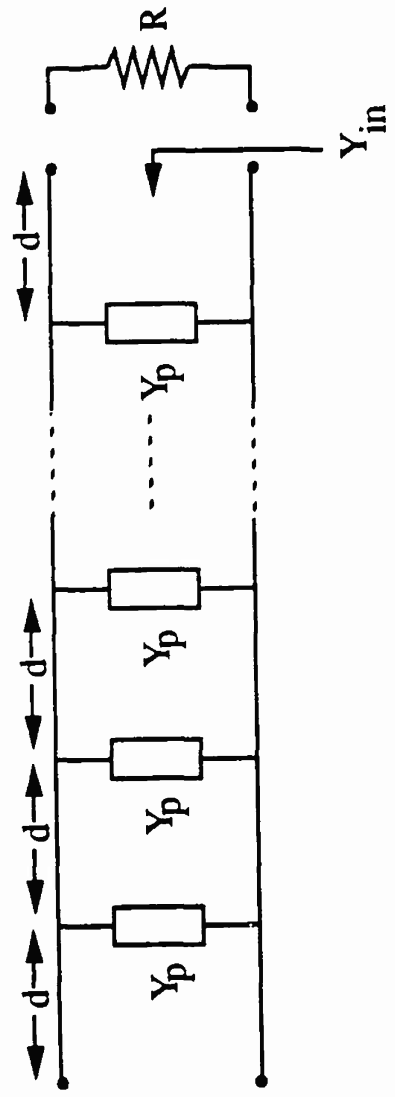


Fig. 5.1 A transmission line loaded periodically with admittance Y_p

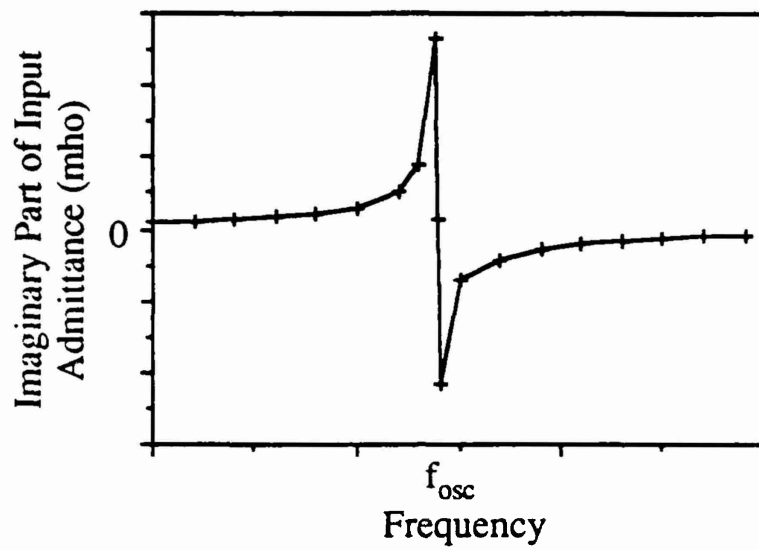


Fig. 5.2 At the oscillation frequency the imaginary part of the admittance seen by looking in to the periodic structure becomes zero.

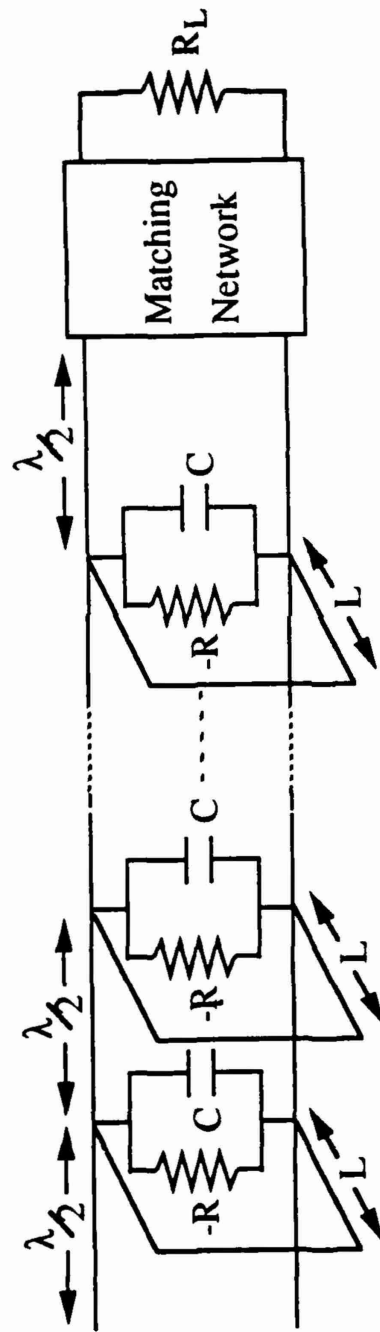


Fig. 5.3 A periodic power combining oscillator. The negative resistance devices are modeled as a parallel- R/C network. The shorted stubs are to compensate the capacitive portion of the device.

structure could also be used to tune out the total capacitance of all the diodes, but in that case, the circuit would be very sensitive to the dimensions of the stub. It should be noted that if the distance between active elements is chosen not to be equal to a half wavelength at the desired oscillation frequency, then even though the oscillation condition can be satisfied (by choosing a proper termination), efficient power combining can not be obtained (in the worst case, no power combining would be achieved). This is because the operating condition for different devices would be different (since the impedance that each device sees would be different) and some active elements would load the power generated by the others.

5.2-Large Signal Impedance Determination

For an accurate design, the large signal impedance of the negative resistance device at the desired oscillation frequency should first be determined. To satisfy the steady state condition for oscillation, the impedance of the passive circuit seen from the active device's port should be equal to negative of the large signal impedance of the device. Therefore, by measuring the impedance of an oscillator circuit seen by the active device (after removing the device) the large signal impedance of the device at the frequency and amplitude of oscillation can be determined. In this experiment, Gunn diodes capable of producing about 10 mW when biased at 8 volts with an efficiency of about 1.2% are used. To measure the large signal impedance, one can construct a test oscillator circuit by connecting a single Gunn diode to a half wave microstrip line resonator (Fig. 5.4). The half wave resonator determines the oscillation frequency. The output of this test structure is connected to a triple stub tuner. After biasing the circuit, the stub tuner is adjusted to obtain the maximum power from the oscillator. The

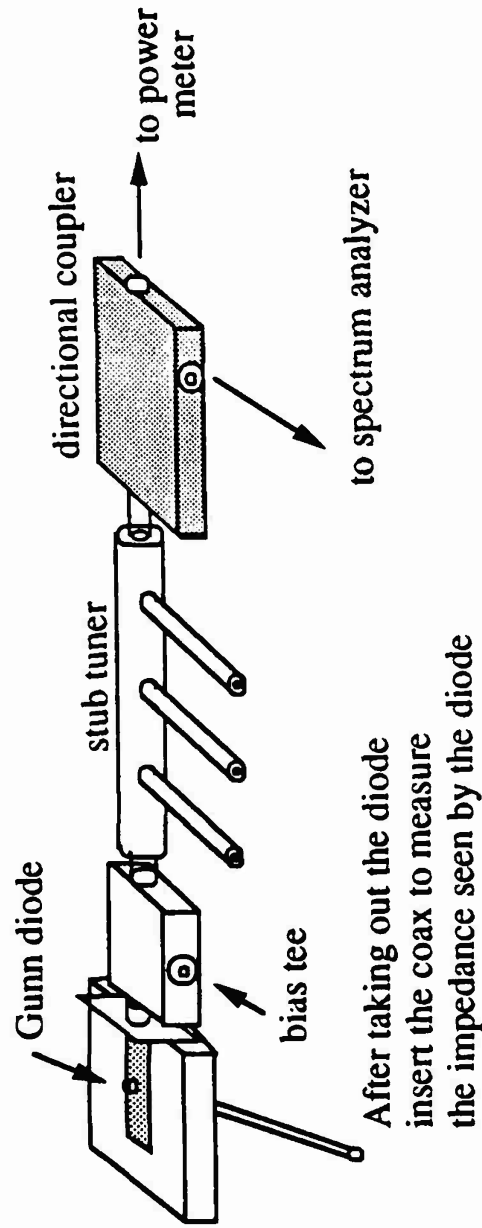
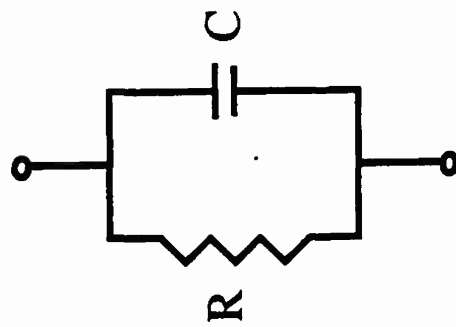


Fig. 5.4 Measurement of large-signal impedance of the Gunn diode

maximum power in this case was is obtained at about 10.5 GHz. Then we disconnect the diode and insert a coaxial cable in its place without disturbing the rest of the circuit. The impedance at the far end of the coax is measured; afterward, the plane of reference is moved to the diode end of the coax. The large signal impedance of the Gunn diode is the negative of the impedance measured. Using this large signal impedance measurement and assuming that the equivalent circuit of the diode consists of a negative resistance in parallel with a capacitance, the values of the negative resistance and the shunt capacitance can be determined. Fig. 5.5 shows the large signal equivalent circuit for a packaged Gunn diode at 10.5 GHz when the diode is biased at 8 volts. It should be remembered that this equivalent circuit is valid only at the oscillation frequency.

5.3-Design Procedure

After the large signal impedance determination of the device at a certain frequency, one can attempt to design the circuit. In general, if we design a circuit such that it provides each Gunn diode the same impedance that was measured using the test oscillator and if we bias the devices at the same voltage, then the diodes should operate under the same condition as the test oscillator. Therefore, the frequency and the power generated from each diode should also be the same. One should note that the stability condition for the new circuit designed based on the large signal analysis can be different from the test oscillator circuit. This is because the stability condition depends on the slope of intersection of the device and circuit line (refer to Chapter 3). Even though the operating point of the test oscillator and the new circuit designed based on the large signal impedance is the same (the point of intersection of the device and circuit lines is the same), the stability condition may be different.



Measurement results:

$$V_{\text{bias}} = 8.5 \text{ v}$$

$$\text{Max power} = 10.47 \text{ mW}$$

$$R = -147 \ \Omega$$

$$C = 0.4 \text{ pF}$$

Fig. 5.5 Large signal equivalent circuit for the packaged Gunn diode at 10 GHz

Referring to Fig. 5.5, since we have already determined the value of the diode's capacitance, we can design shunt stubs such that they compensate the capacitance of each diode. What we are left with are several negative resistances periodically spaced by $\lambda/2$. It can be shown that the impedance each diode sees is the same as the negative of the large signal impedance we measured if the periodic structure is terminated properly. For an N diode oscillator, the proper termination impedance is $1/N$ times the negative of the resistance of a single diode. The proper termination impedance can be transformed to 50 ohms using a quarter-wave transformer. As the number of the diodes increases the value of the proper termination which satisfies the oscillation condition decreases. Impedance matching between the proper termination and 50 ohms can put a limit to the number of the diodes that can be used in the periodic structure. The maximum number of diodes that can be used to get a high power combining efficiency depends on the type of the diode (its large signal impedance) and the characteristics of the substrate and the transmission line. Figure 5.6 shows a drawing of the three-diode power combiner.

5.4-Experiment and Results

Based on the large signal impedance of the Gunn diodes, two, three, five and six-diode power combining oscillators were designed and constructed. The structures were fabricated on a woven Teflon™ substrate with a dielectric constant of 2.5 and thickness of 32 mils. The structures were biased using a bias tee connected to their output terminals. After a 10 second warm up period, the Gunn oscillators injection lock to each other. When phase locking is achieved, the output power can be maximized by fine adjustment of the bias voltage. Injection locking was maintained in

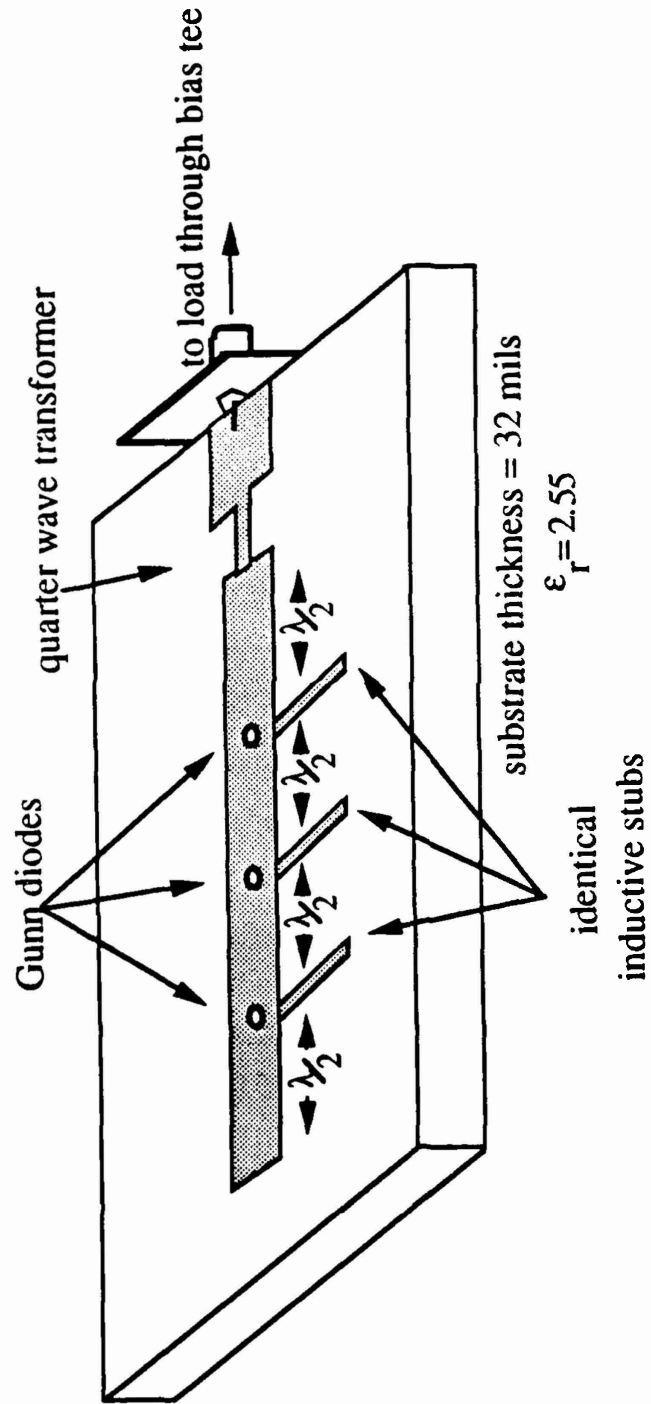


Fig. 5.6 Three Gunn diode periodic power combining oscillator

spite of large variations in the bias voltage. For example, in the case of the five-diode power combiner, bias voltage variations greater than ± 2 volts were required to cause the oscillators to lose phase lock. It should be pointed out that the diodes were not selected to have matched characteristics. Using a power meter it was observed that the output power was maximum if all the Gunn oscillators were injection locked together.

The one-diode planar oscillator produced maximum power of about 10.47 mW at 10.5 GHz with an efficiency of about 1.2%. Results obtained from different power combining structures are shown in Table 5.I. The radiation from all the combiners was at least 17 dB below the power absorbed by the load. Except in the case of the six-diode power combiner, combining efficiencies were all more than 100 %. This is believed to be due to the fact that better matching to 50 ohms was achieved compared to the single Gunn diode oscillator. The maximum power combining efficiency was obtained from the three diode power combiner. This is what one expects to observe. Looking at the equivalent circuit for the Gunn diode we see that the value of the negative resistance is -147Ω . In the case of the three diode combiner, three diodes are in parallel and the termination resistance which satisfies the oscillation condition is about 50Ω . This means that there is no need for a quarter-wave transformer for impedance matching and therefore the power combining efficiency is maximum since we can avoid losses that could be introduced by the matching circuit.

The dependence of the oscillation frequency on the bias voltage was investigated. The results are shown in Fig. 5.7. In general it seems that the dependence of the oscillation frequency on the bias voltage is not a function of the number of diodes in the structure.

N	power (mW)	frequency (GHz)	bias voltage	combining efficiency (%)
1	10.47	10.5	8.5	-----
2	25.0	10.2	8.6	119 %
3	39.8	10.0	8.5	126.7 %
5	63.4	9.5	9.8	121 %
6	56.2	9.9	9.0	89.5 %

Table 5.1 Characteristics of various power combining oscillators. N is the number of diodes used in the structure.

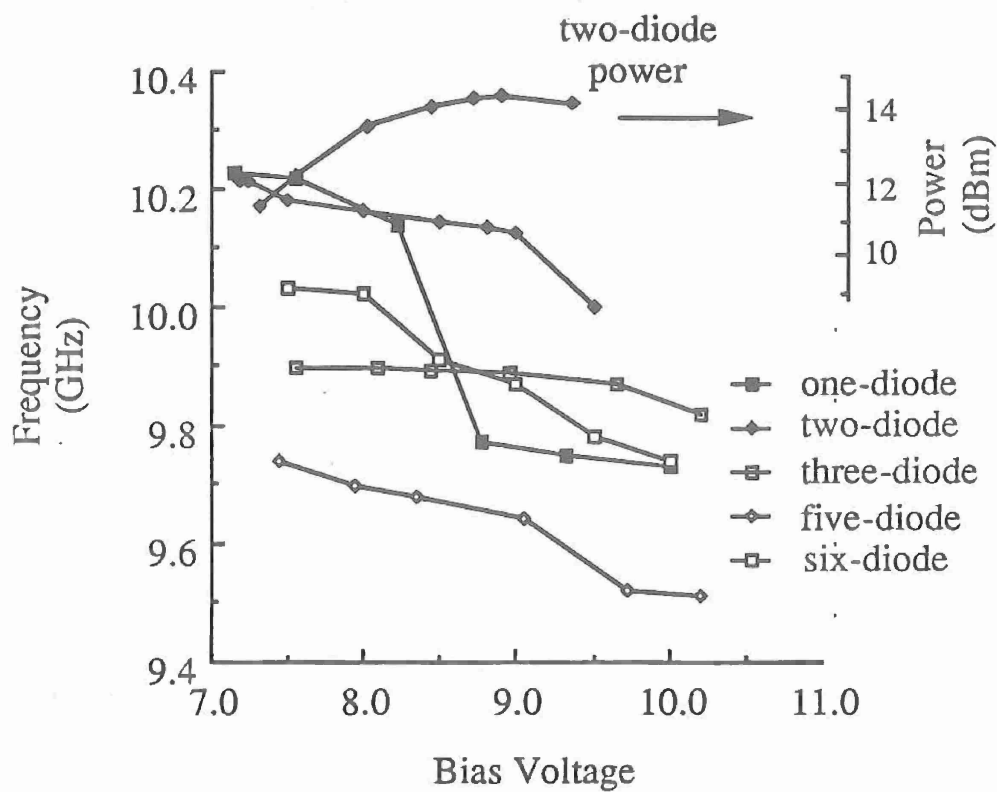


Fig. 5.7 Variation of the oscillation frequency with bias voltage. Also, the power generated by a two-diode combiner as a function of bias voltage is shown.

The second harmonic generated by the combiners was also investigated. For the single Gunn diode oscillator the second harmonic was 21 dB below the fundamental. In the case of two, three, five and six-diode combiners the second harmonic was 18.5, 16, 23.3, and 15 dB below the fundamental.

5.5-Conclusion

In this chapter, a simple method of power combining was introduced. In this technique, the periodicity of the structure determines the oscillation frequency, therefore eliminating the need for an external resonator. Consequently, the simplicity of the structure makes it compatible with monolithic fabrication. This structure can be used to combine power generated from several QWITT diode oscillators.

Using low power Gunn diodes, two, three, five and six-diode distributed power combining oscillators in the X-band were designed and fabricated. The generated powers for the case of the two, three, five, and six-diode combiners were 2.4, 3.8, 6.1 and 5.4 times the power produced by a single diode oscillator, respectively. The frequency dependence of all the power combiners on the bias voltage variation seemed to be independent of the number of the diodes. It was observed that, when injection locking was achieved, it was maintained over relatively large variations of the bias voltage.

CHAPTER 6

SECOND HARMONIC QUASI-OPTICAL POWER COMBINERS AND TRANSCEIVERS

At millimeter and sub-millimeter wave frequencies, solid state devices have limited capability to produce microwave energy. At these frequency ranges, the efficiency of solid state devices drops dramatically. In order to obtain higher power, it is very desirable to combine the power generated from many single solid state oscillators [18]. In addition, there is always a limit to the frequency at which a solid state oscillator can operate. In that limit, the negative resistance of the device becomes so small that it can not compensate the resonator's loss. In this case power combining alone can not help. One way to generate millimeter and sub-millimeter wave frequencies is to use two terminal solid-state devices as harmonic generators. Even though solid state devices do not exhibit negative resistance above a certain range of frequencies, because of device nonlinearities, higher harmonics are being generated. Through proper circuit design, harmonic generation can be enhanced and then filtered out for use. One problem with this method is the low conversion efficiency. Here again we can take advantage of different power combining techniques [23]. In general, at millimeter wave frequencies spatial power combining techniques are preferred since guiding structures are lossy [24]. Since the nonlinearity of negative resistance devices is maintained at higher harmonics, they can also be used as self-oscillating harmonic mixers. This type of approach can simplify the construction of transceiver modules and hence reduce their size and cost.

In this chapter, for the first time, a periodic second harmonic spatial power combining structure is discussed. A periodic structure designed for fundamental power combining is described in Chapter 5 [25]. The present circuit takes advantage of the periodicity of the structure to determine the frequency of oscillation and consequently the frequency of the second harmonic. In this method, phase locking is accomplished without using an external resonator such as a Fabry-Perot resonator [26, 27]. Therefore, this circuit is planar and suitable for use in monolithic integrated circuits. Since the fundamental frequencies are phase locked to each other, and assuming that all the devices are similar, the second harmonics generated should have the same phase. An antenna array can be designed to radiate at only the desirable harmonic frequency. Also, a modified version of the circuit which acts as a second harmonic quasi-optical transceiver is presented. In this experiment, an array of microstrip patch antennas is used for transmitting and receiving purposes. For receiving, the received RF power from the antenna array is mixed down with the second harmonic generated from the Gunn devices. The IF power output is through a lowpass filter.

6.1-Theory

Simulation of the second harmonic generation was considered by Solbach [28]. As was also discussed in Chapter 2, the current-voltage relationship for the active device can be described by a power series.

$$I = a_1 V + a_2 V^2 + a_3 V^3 \quad (6.1)$$

Also, it is mentioned in Chapter 2 that the linear coefficient a_1 has to be a negative number for a negative resistance device and it represents the small signal

negative conductance of the active element. The value of the cubic term a_3 is determined by the maximum available power from the device. The inclusion of quadratic term shifts the I-V curve to an unsymmetric point which affects the harmonic generation. The model used to describe the second harmonic operation of a negative resistance device like a Gunn diode is shown in Fig. 6.1. A frequency multiplexing network represents the fundamental as well as second harmonic behavior of a second harmonic generator. The circuit is divided into two parts. One is the resonator circuit which determines the fundamental frequency of oscillation and the second part represents the load that appears across the diode's terminals at the second harmonic. Steady state analysis of such a circuit is described in the following.

We assume that the voltage across the active device contains only fundamental and second harmonic components and all the higher harmonics are set to zero.

$$V = v_1 e^{-j\omega t} + v_2 e^{-j\phi} e^{-j2\omega t} \quad (6.2)$$

The phase difference between the fundamental and the second harmonic voltage is represented by ϕ . By substituting the above equation into Eq. 6.1, we can calculate the current through the active device. All the harmonics higher than second are neglected.

$$I_1 = a_1 v_1 + a_3 \left(\frac{3v_1^3}{4} + \frac{3v_1 v_2^2}{2} \right) + a_2 v_1 v_2 \cos \phi + j a_2 v_1 v_2 \sin \phi \quad (6.3)$$

$$I_2 = a_1 v_2 + a_3 \left(\frac{3v_2^3}{4} + \frac{3v_2 v_1^2}{2} \right) + a_2 \frac{v_1^2}{2} \cos \phi - j a_2 \frac{v_1^2}{2} \sin \phi \quad (6.4)$$

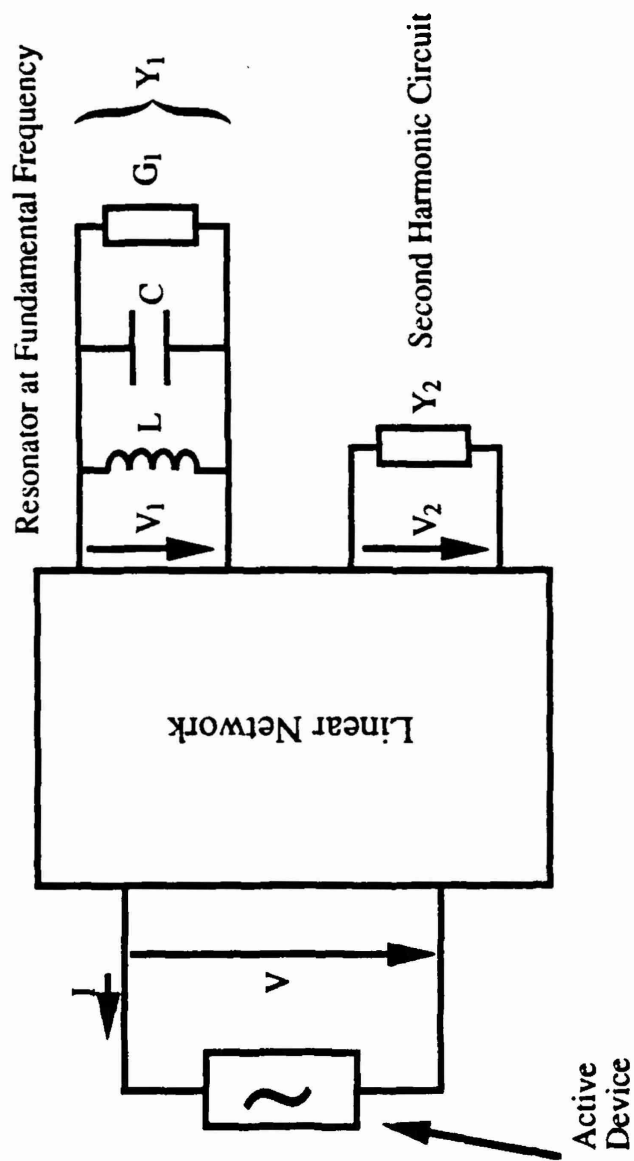


Fig. 6.1 Equivalent circuit representation of a second harmonic oscillator

In the harmonic generator circuit (Fig. 6.1) the following two nodal equations should be satisfied:

$$I_1 + V_1 Y_1 = 0 \quad (6.5)$$

$$I_2 + V_2 Y_2 = 0 \quad (6.6)$$

The fundamental mode oscillator can be analyzed by letting $Y_2 = \infty$. From solving Eq. 6.5 we can determine the frequency of oscillation ($\omega = 1/\sqrt{LC}$) and the relation between the output power and the load conductance which is discussed in Chapter 2.

To analyze the second harmonic mode of operation we let $G_1 = 0$. This means no power is dissipated at the fundamental frequency (in order to maximize the efficiency in the harmonic generation mode it is desirable not to have any power dissipation at the fundamental frequency). From Eqs. 6.3, 6.4, 6.5 and 6.6 we can get

$$a_1 + a_2 v_2 \cos \phi + a_3 \left(\frac{3v_1^2}{4} + \frac{3v_2^2}{2} \right) + ja_2 v_2 \sin \phi + j \left(\omega C - \frac{1}{\omega L} \right) = 0 \quad (6.7)$$

$$a_1 + a_2 \frac{v_1^2}{2v_2} \cos \phi + a_3 \left(\frac{3v_2^2}{4} + \frac{3v_1^2}{2} \right) + ja_2 \frac{v_1^2}{2v_2} \sin \phi + Y_2 = 0 \quad (6.8)$$

To facilitate our discussion and also for second harmonic power combining purposes (it will be clear in the next section), we let the load at the second harmonic be purely real $Y_2 = G_2$. This implies that $\sin \phi = 0$ (from Eq. 6.8). This means that there is no phase difference between the fundamental and second harmonic voltages. Also from Eq. 6.7 we can see that the oscillation frequency is determined by the fundamental mode oscillator circuit ($\omega = 1/\sqrt{LC}$).

6.2-Circuit Description

The periodic second harmonic spatial power combining oscillator is shown in Fig. 6.2. A microstrip transmission line is loaded periodically with four Gunn diodes with a distance equal to approximately a half guide wavelength at the fundamental frequency of oscillation (f_1). The line dispersion is neglected and it is assumed that the guided wavelength at the fundamental frequency (λ_{g1}) is equal to twice the guided wavelength at the second harmonic (λ_{g2}). The voltage waveforms across the power combining structure at the fundamental and the second harmonic are shown in Fig. 6.3. It is assumed that the diodes' characteristics are exactly the same and that the doubling action does not contribute any phase component to the second harmonic waveform. This assumption is valid if the value of the impedance seen by the diode at the second harmonic is purely resistive and no power is dissipated at the fundamental frequency (the real part of the impedance seen by the diode at the fundamental frequency is zero) (refer to Section 6.1).

At the second harmonic, the periodicity of the structure will be equal to approximately a full wavelength. Because this satisfies the leaky wave stopband condition, broadside radiation will result. Also the structure is connected to four microstrip patch antennas to compose an antenna array. The distance between each array element is equal to the periodicity of the main structure. The patch antennas are resonant at the second harmonic (f_2) and therefore only the second harmonic can be efficiently radiated. As shown in Fig. 6.3, all the antennas are in phase. Since the diodes are about a half wavelength apart at the fundamental frequency, the radiated

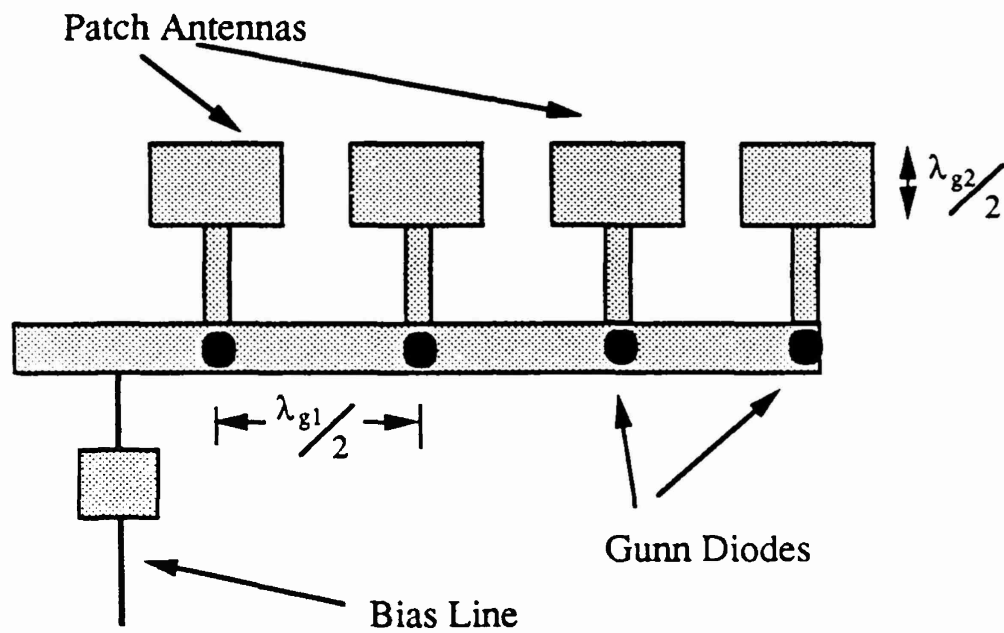


Fig. 6.2 Diagram of a four diode spatial second harmonic power combiner

λ_{g1} is the guide wavelength at fundamental frequency

λ_{g2} is the guide wavelength at fundamental frequency

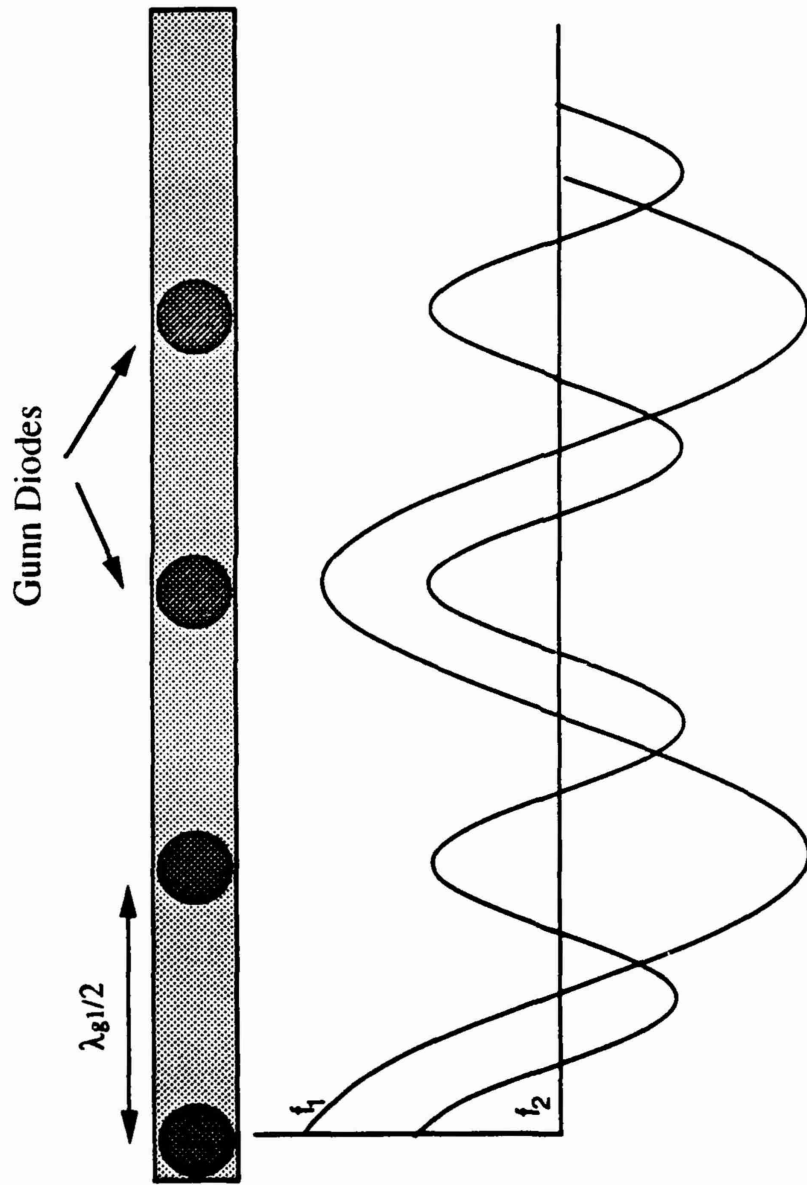


Fig. 6.3 Voltage waveforms at the fundamental and the second harmonic across the power combining structure

power from discontinuities at f_1 should have its null in the broadside direction, so the interference between the fundamental and the second harmonic is minimal.

6.3-Design

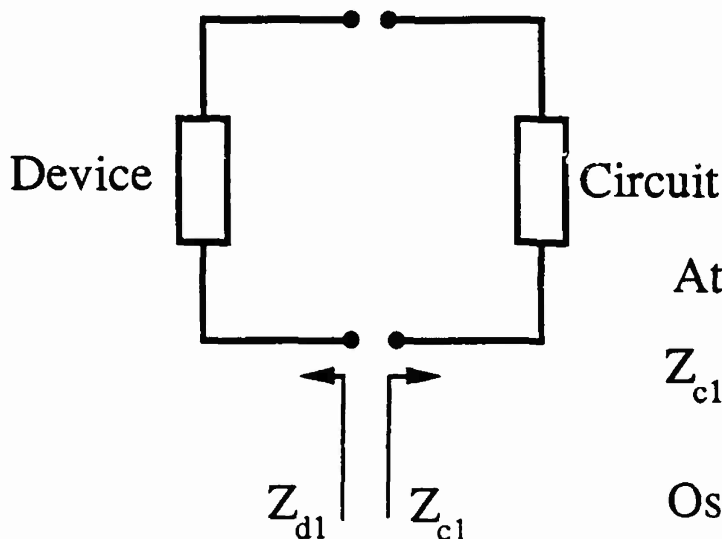
In this experiment, the author used low power packaged Gunn diodes designed to operate at the X-band. The circuits were fabricated using a Duroid™ 5880 substrate with a thickness of 20 mils and a relative dielectric constant of 2.2. The first step is to determine the impedance which the negative resistance device should see at the fundamental and the second harmonic in order to generate maximum power at the second harmonic. The measurement set up is shown in Fig. 5.4. A single microstrip Gunn diode oscillator is constructed. A half-wave microstrip resonator is used to determine the fundamental frequency of oscillation. The circuit is connected to a spectrum analyzer through a triple stub tuner. By adjusting the stub tuner and trimming the microstrip circuit, the power generated at the second harmonic can be maximized. Then the Gunn diode was removed from the circuit without introducing any other change. A piece of semi-rigid coax is then connected to the circuit in place of the Gunn diode. The impedance of the circuit at the fundamental (Z_1) and at the second harmonic (Z_2) is measured using a network analyzer after transferring the plane of reference to the end of the coaxial cable. The impedances that are measured are those that should be seen by the Gunn diode in order to generate the maximum second harmonic at a particular frequency. At the fundamental frequency of oscillation, the resonance condition should be satisfied. Therefore the large signal impedance of the Gunn diode at the fundamental frequency is $-Z_1$. Also since Z_2 is the impedance to which the Gunn diode delivers maximum power, the maximum power transfer condition should be

satisfied and so the impedance of the diode at the second harmonic is equal to the complex conjugate of Z_2 (Fig. 6.4). In this experiment, the fundamental frequency at which the Gunn diode generated maximum second harmonic is 9.3 GHz. The impedances seen by the diode are $Z_1 = 5 + j35 \Omega$ and $Z_2 = 20 + j3 \Omega$. Since the impedance Z_1 is mostly reactive, power at the fundamental is not absorbed, and the interaction between the fundamental and the device nonlinearities is maximized. Also, the value of Z_2 is mostly, real therefore the impedances that appear at the diodes terminals at the fundamental and the second harmonic approximately satisfy the requirements that were discussed in Section 6.1. The maximum power obtained from a single Gunn diode oscillator at 18.6 GHz (f_2) was about 5.7 dBm.

In order to provide the diodes the proper impedances (Z_1 and Z_2), the length and the impedance of the feed line to the antennas, the impedance of the main line, and, slightly, the periodicity of the structure are adjusted so that the impedance looking at each diode port is Z_1 and Z_2 at f_1 and f_2 respectively. Since the periodicity of the structure is one half of the guide wave length at the fundamental frequency and one guide wavelength at the second harmonic, after providing one of the diodes the correct impedances the others will also see the correct impedances. The circuit design was done using the Touchstone™ microwave circuit analysis program.

The patch antennas were designed based on the transmission line model for microstrip patch antennas [29]. After designing the patch antennas their impedances were measured using the HP8510 network analyzer. The theory and measurement were in good agreement. Therefore, the theoretical values for the impedance were used throughout the design procedure.

At the fundamental frequency:



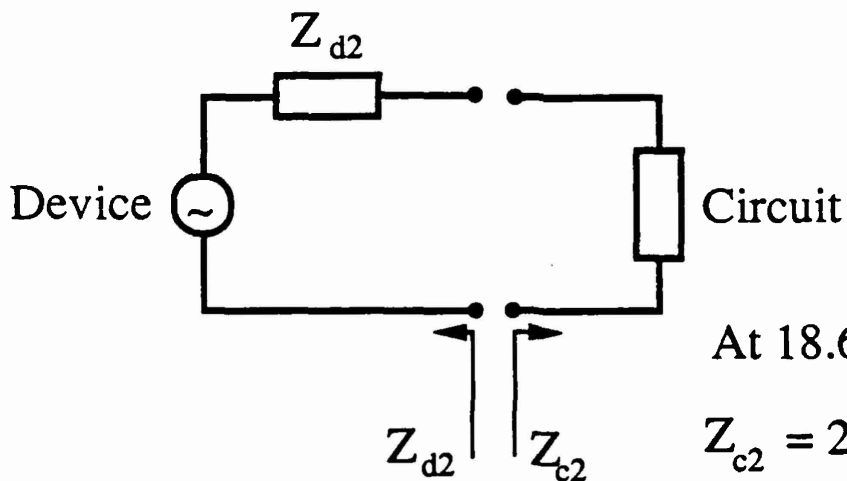
At 9.3 GHz:

$$Z_{c1} = 5 + j 35 \Omega$$

Osc. Condition:

$$Z_{d1} = - Z_{c1}$$

At the second harmonic:



At 18.6 GHz:

$$Z_{c2} = 20 + j 3 \Omega$$

Max. Power Transfer:

$$Z_{d2} = Z_{c2}^*$$

Fig. 6.4 Determination of the large signal impedance of a packaged Gunn diode at the fundamental and second harmonic frequencies. The circuit is optimized for maximum second harmonic generation.

6.4-Experiment

A four diode spatial power combining structure was designed and fabricated (Fig. 6.5). The antenna radiation pattern is shown in Figs. 6.6 and 6.7. For quasi-optical oscillators, one may define an effective radiated power (ERP) as the power needed to drive an isotropic radiator to provide the same power density transmitted by the quasi-optical oscillator at a certain direction. The ERP is measured by comparing the output of a standard gain horn driven with a known RF power to that of the quasi-optical oscillator [30] also, an isotropic conversion efficiency can be defined as the ratio of the ERP to the dc power consumed by the quasi-optical oscillator [31]. The effective radiated power (ERP) for the four diode second harmonic power combiner was determined to be 25.7 dBm. The isotropic conversion efficiency was 10.2%. The cross polarization was 17 dB below the peak power in the broadside direction. The power radiated at fundamental frequency was 15 db below the power at the second harmonic measured in the broadside direction [32].

In order to determine the power combining efficiency of this structure, the following measurement was performed. The maximum power generated by a single diode oscillator (5.7 dBm) was injected to a single patch antenna. The effective radiated power was measured to be 13.4 dBm. This shows that the ERP from the four diode harmonic combiner (25.7 dBm) is about sixteen times the ERP of a single diode. The extra factor of four is due to the array factor.

The performance of the four diode power combiner as a mixer was also tested. For quasi-optical transceivers one can define an isotropic receiver gain as the ratio of IF power to that of an isotropic receiver with 100 percent RF-IF conversion efficiency

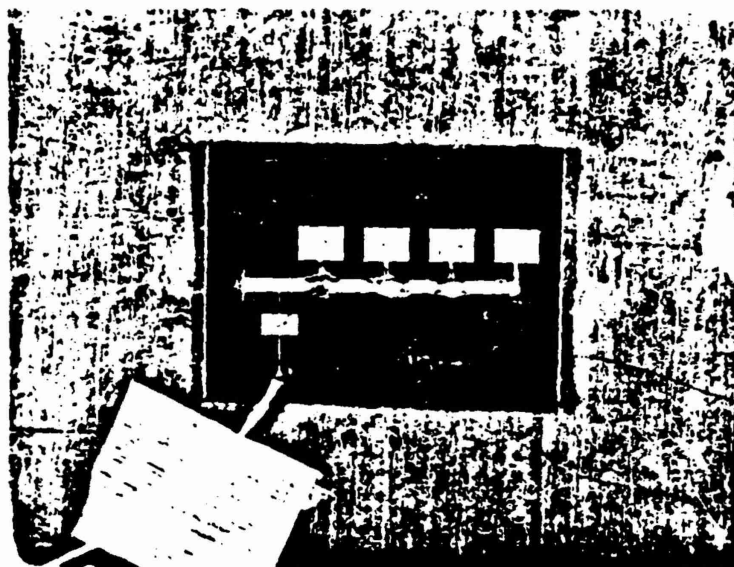


Fig. 6.5 Photograph of a second-harmonic four-diode power combining structure

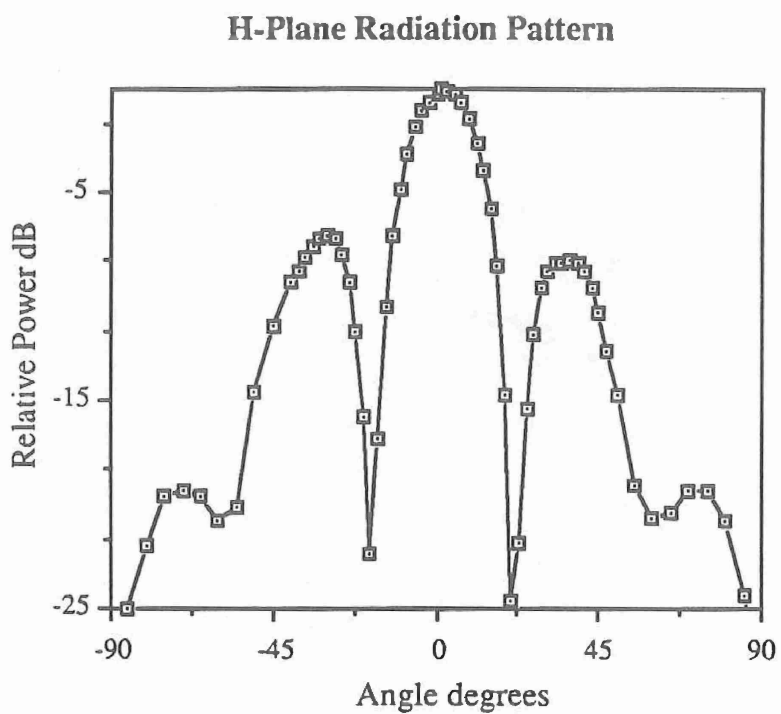


Fig. 6.6 The H-plane radiation pattern of the four-diode harmonic combiner.

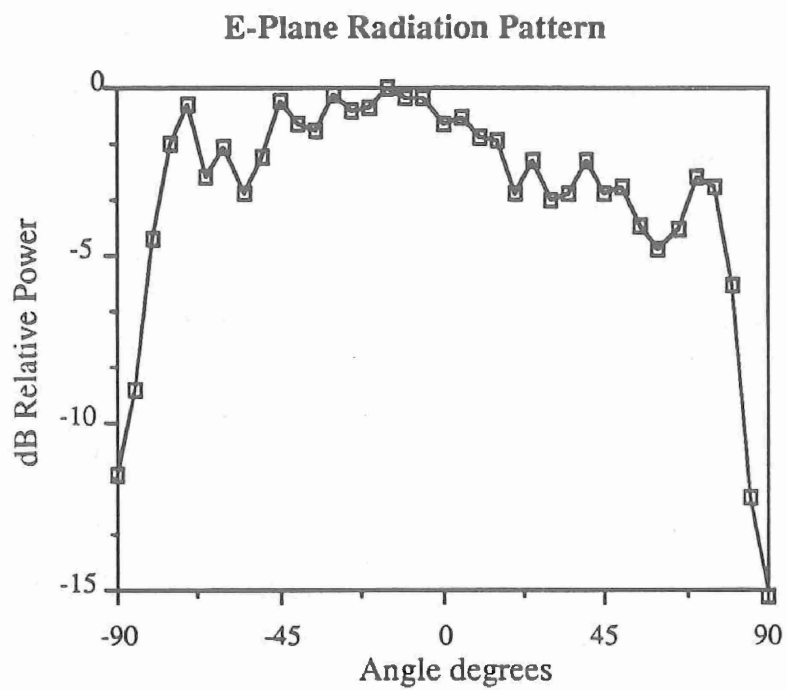


Fig. 6.7 The E-plane radiation pattern of the four-diode harmonic combiner.

[33]. The maximum isotropic receiver gain at IF of 100 MHz was measured to be 6 dB at a bias voltage of 11 Volts. The IF bandwidth in this case was about 20 MHz. In general, the condition for the optimum power combining does not coincide with the condition for the optimum mixing efficiency. In order to improve the receiving performance of the quasi-optical transceiver, the active devices were isolated from each other at the second harmonic.

In order to isolate the active devices from each other, a low-pass filter can be inserted between each pair of them. The cutoff frequency of the active filter is chosen to be higher than the fundamental frequency of oscillation so that the diodes are still injection locked to each other at the fundamental frequency of oscillation. As far as mixing is concerned, different devices act as isolated down converters and IF signals generated by them are added to each other. This is based on the assumption that the devices' characteristics are exactly the same.

A two diode second harmonic transceiver with the low-pass filter is shown in Fig. 6.8. Each diode is connected to a half-wave resonator which determines the fundamental frequency of oscillation. The low-pass filter had a cutoff frequency of 10 GHz. The two Gunn oscillators are phase locked to each other at the fundamental frequency of 8.5 GHz. The electrical length of the filter structure is one wavelength at the fundamental frequency. The low-pass filter isolates the two Gunn diodes from each other at the second harmonic (17 GHz). It should be mentioned that no attempt was made to provide any IF matching for the transceiver.

The receiving and transmitting antenna patterns are shown in Figs. 6.9 and 6.10 respectively. The receiving pattern is determined by measuring the IF output power of

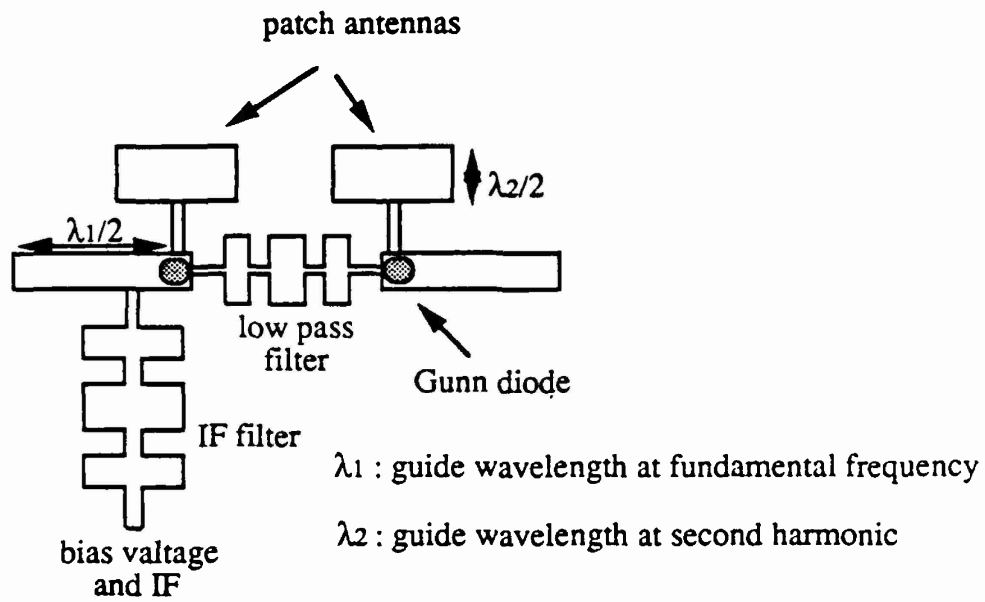


Fig. 6.8 A second harmonic transceiver

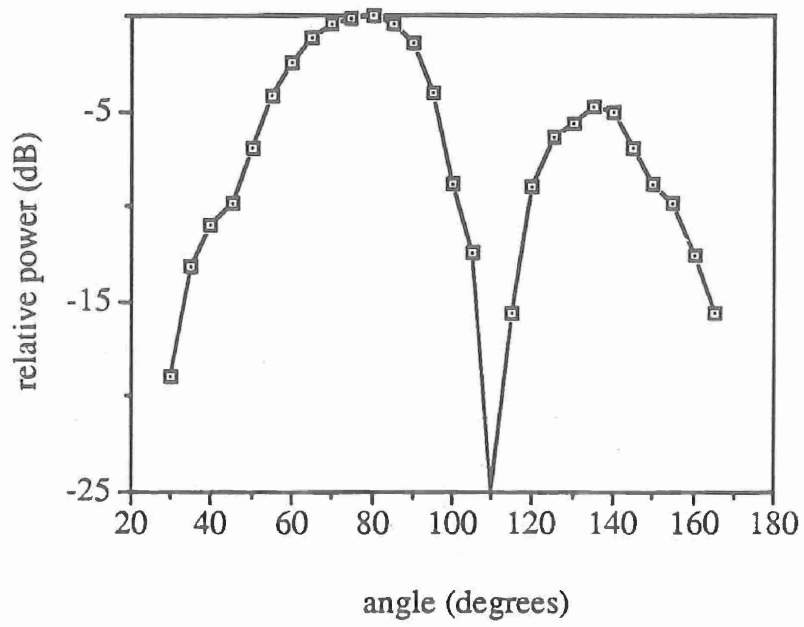


Fig. 6.9 Receiving H-plane radiation pattern

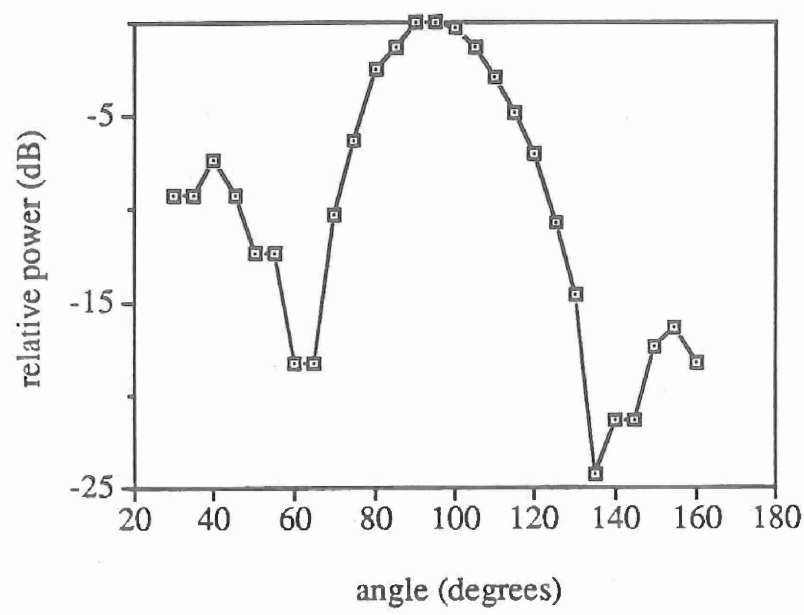


Fig. 6.10 Transmitting H-plane radiation pattern

the receiver. The positions of the peaks and nulls of the receiving antenna pattern are shifted as compared to the transmitting antenna pattern. The difference between receiving and transmitting patterns is due to the fact that the two diodes are not exactly matched, therefore, the phase of the IF signal generated from each device is not the same. This problem is expected to be overcome in monolithic circuit fabrication, since all the devices on the same chip should have very similar characteristics. The ERP of the two diode transceiver was determined to be equal to 13 dBm at 17 GHz. The receiving isotropic conversion gain was 10 dB. The IF frequency was about 100 MHz and the bias voltage was 10 volts [34].

6.5-Conclusion

A periodic second harmonic spatial power combining oscillator is presented. The oscillators are phase locked at the fundamental frequency. The power is combined in free space. This power combining method makes the use of external resonator circuits unnecessary. This type of circuit structure is compatible with monolithic fabrication. The effective radiated power from a four diode second harmonic combiner is about sixteen times the ERP of a single harmonic generator.

A second harmonic two diode transceiver was also demonstrated. In this case the power combining structure can also function as a receiver. These types of structures are advantageous in microwave and millimeter wave applications, since a single circuit can perform several different functions. This structure can easily be expanded by using more diodes to generate higher powers.

CHAPTER 7

CONCLUSIONS

In this dissertation, the measurement of the small signal microwave impedance of the QWITT diode is discussed. The calculated results from a theoretical model of the QWITT diode are in close agreement with the experimental values. It was concluded, that due to the large parasitic series resistance, the QWITT diodes that were tested could not oscillate in the millimeter wave region. Millimeter wave operation could be achieved by reducing the series resistance due to the ohmic contacts by an order of magnitude or more. Also, results of the first planar circuit implementation of a quantum well oscillator are presented. There is considerable room for optimization of both the oscillator circuit and physical device parameters to maximize the oscillator output power. In order to design planar QWITT diode oscillators at millimeter wave frequencies whisker contacts should be eliminated. This can be done by fabricating planar QWITT diodes. In this case, coplanar waveguide structures can be used for circuit design.

Two types of self oscillating QWITT diode mixers are presented, one in waveguide and the other in a planar configuration. The waveguide mixer operates in the third harmonic and the planar mixer operates in the fundamental mode of conversion. Both of these mixers can achieve conversion gain.

In order to improve the millimeter wave power level generated by several negative resistance devices like the QWITT diode, a periodic power combining structure is introduced. This power combiner has a simple structure. Since no external resonator is used, the circuit is compatible with monolithic fabrication. To demonstrate

this idea, several Gunn diodes are used. In some cases, power combining efficiencies higher than 100% are obtained.

The QWITT diode is a highly nonlinear device, therefore it can be used as a harmonic generator. Since the power generated at higher harmonics drops rapidly, a power combining method is presented which is designed to combine the second harmonic power generated by several negative resistance devices. The power combining is performed using quasi-optical techniques. The circuit is periodic and the periodicity of the structure determines the fundamental frequency of oscillation. Because of its structure, it can be fabricated in monolithic form. This type of circuit can also be used as a quasi optical transceiver module.

REFERENCES

- [1] H. Gronqvist, A. Rydberg, H. Hjelmgren, H. Zirath, E. Kollberg, J. Soderstrom and T. Andersson, "A millimeter wave quantum well diode oscillator," Proc. of the 18th European Microwave Conference, pp. 370-375, Stockholm, Sweden, Sep. 1988.
- [2] E.R. Brown, W.D. Goodhue, and T.C.L.G. Sollner, "Fundamental oscillations up to 200 GHz in resonant tunneling diodes and new estimates of their maximum oscillation frequency from stationary-state tunneling theory," J. Appl. Phys., vol. 64, pp. 1519-1529, Aug. 1988
- [3] E.R. Brown, T.C. L.G. Sollner, C.D. Parker, W.D. Goodhue and C.L. Chen, "Oscillations up to 420 GHz in GaAs/AlAs resonant tunneling diodes," Appl. Phys. Lett. 55, pp. 1777-1779, Oct. 1989
- [4] V.P. Kesan, D.P. Neikirk, B.G. Streetman and P.A. Blakey, " A new transit time device using quantum well injection," IEEE Elec. Device Lett., vol. EDL-
- [5] A. Mortazawi, D.R. Miller, D.P. Neikirk and T. Itoh, "Small signal measurements of the microwave impedance of QWTTT diodes," to be presented at the 20th European Microwave Conf., Sep. 1990
- [6]. J.M. Gering, D.A. Crim, D.G. Morgan, P.D. Coleman, W. Kopp and H. Morkoc, "A small signal equivalent-circuit model for GaAs-Al_xGa_{1-x}As resonant tunneling heterostructures at microwave frequencies," J. Appl. Phys., pp. 271-276, Jan. 1987

- [7] V.P. Kesan, D. P. Neikirk, T. D. Linton, P. A. Blakey, and B. G. Streetman, "Influence of transit time effects on the optimum design and maximum oscillation frequency of quantum well oscillators," *IEEE Trans. Electron Devices* ED-35, pp. 405-413, Apr. 1988
- [8] D.R. Miller, V.P. Kesan, R.L. Rogers, C.M. Maziar, and D.P. Neikirk, "Time dependent simulation of the quantum well injection transit time diode," *Proc. of the 13th Int. Conf. on Infrared and mm Waves*, pp. 5-6, Dec. 1988
- [9] K. Kurokawa, "Some basic characteristics of broad band negative resistance oscillator circuits," *Bell Sys. Tech. J.*, vol. 48, no. 6, pp. 1937-1955, July 1969
- [10] D.J. Esdale and M.J. Howes, "A reflection coefficient approach to the design of one port negative impedance oscillators," *IEEE Trans. Microwave Theory Tech.*, vol. MTT-29, pp. 770-776, Aug. 1981
- [11] B. Van der Pol, "The nonlinear theory of electric oscillations", *Proc. IRE*, vol 22, pp. 1051-1086, 1934
- [12] T. Bercelli, *Nonlinear Active Microwave Circuits*, Amsterdam: Elsevier, 1987, Ch. 2
- [13] V.P. Kesan, A. Mortazawi, D.R. Miller, T. Itoh, B.G. Streetman and D.P. Neikirk, "Microwave frequency operation of quantum well injection transit time (QWITT) diode, " *Electron. Lett.*, vol 24, no. 24, p 1473-1473, Nov. 1988

- [14] V.P. Kesan, A. Mortazawi, D.R. Miller, V.K. Reddy, D.P. Neikirk and T. Itoh, "Microwave and millimeter wave QWITT diode oscillator," *IEEE Trans. Microwave Theory Tech.*, vol. MTT-37, pp. 1933-1941, Dec. 1989
- [15] T.C.L.G. Sollner, E.R. Brown and H.Q. Lee, "Microwave and millimeter wave resonant tunneling devices," *Lincoln Lab. J.*, vol. 1, no 1, pp. 89-106, Spring 1988
- [16] A. Mortazawi, V.P. Kesan, D.P. Neikirk and T. Itoh, "A periodic monolithic millimeter wave quantum well oscillator," *Proc. of the 13th Int. Conf. on Infrared and mm waves*, PP. 47-48, Dec. 1988
- [17] V.P. Kesan, A. Mortazawi, D.P. Neikirk and T. Itoh, "Microwave and millimeter wave QWITT diode oscillator," *IEEE MTT-S Int. Microwave Symp. Dig.*, vol. 1, pp. 487-490, June 1989
- [18] K. Chang and C. Sun, "Millimeter-wave power-combining techniques," *IEEE Trans. Microwave Theory Tech.*, vol. MTT-31, pp. 91-107, Feb. 1983
- [19] K. Kurokawa, "The single cavity multiple-device oscillator," *IEEE Trans. Microwave Theory Tech.*, vol. MTT-19, pp. 793-801, Oct. 1971
- [20] Y. Fukuoka and T. Itoh, "Millimeter-wave travelling-wave Impatt diode," *Microwave Laboratory Report No. 84-7*, The University of Texas at Austin
- [21] B. Bayraktaroglu and H. D. Shih, "High-power 60 GHz monolithic GaAs Impatt diodes," *Electron Lett.*, 22, pp. 562-563, May 1986

- [22] V. P. Kesan, A. Mortazawi, D. P. Neikirk, T. Itoh, "Monolithic millimeter-wave oscillator using a transmission line periodically loaded by QWITT diodes," *Electron. Lett.*, 24, pp. 666-667, May 1988
- [23] H. Barth, "A wideband, backshort-tunable second harmonic W-band Gunn oscillator," *IEEE MTT-S Int. Microwave Symp. Dig.*, pp. 334-337, 1981
- [24] J. W. Mink, "Quasi-optical power combining of solid-state millimeter-wave sources," *IEEE Trans. Microwave Theory Tech.*, vol. MTT-34, pp. 273-279, Feb. 1986
- [25] A. Mortazawi and T. Itoh, "A periodic planar Gunn diode power combining oscillator," *IEEE Trans. Microwave Theory Tech.*, vol. MTT-38, Jan. 1990
- [26] Z.B. Popovic, M. Kim and D.B. Rutledge, "Grid oscillators," *International Journal of Infrared and Millimeter Waves*, vol. 9, pp. 1507-1514, Nov. 1988
- [27] S.L. Young and K.D. Stephan, "Stabilization and power combining of planar microwave oscillators with an open resonator," *IEEE MTT-S Int. Microwave Symp. Dig.*, pp. 185-188, 1987
- [28] K.Solbach, "Simulation study of harmonic oscillators," *IEEE MTT Trans. Microwave Theory Tech.*, vol. MTT-30, pp. 1233-1237, Aug. 1982
- [29] J.R. Tames, P.S. Hall and C. Wood, *Microstrip Antenna Theory and Design*, Peter Peregrinnus Ltd.,1981, London

- [30] J. Birkeland, Planar Integrated Circuits for Microwave Transmission and Reception, Ph.D. Dissertation, The University of Texas at Austin, Aug. 1989
- [31] J. Birkeland and T. Itoh, "Planar FET oscillators using periodic microstrip patch antennas," IEEE Trans. Microwave Theory Tech., vol. MTT-37, pp. 1232-1236, Aug. 1989
- [32] A. Mortazawi and T. Itoh, "A second harmonic spatial power combining oscillator," IEEE MTT-S, Int. Microwave Symp. Dig., pp. 1213-1216, May 1990
- [33] K. Stephan and T. Itoh, "A planar quasi-optical subharmonically pumped mixer characterized by isotropic conversion loss," IEEE MTT Trans. Microwave Theory Tech., vol. MTT-32, pp. 97-102, Jan. 1984
- [34] A. Mortazawi, K. Kawasaki and T. Itoh, "A periodic second harmonic spatial power combining oscillator," submitted to IEEE Trans. Microwave Theory Tech.